Examples of Failure Analysis of Multiphase Materials

Eligiusz Postek

Institute of Fundamental Technological Research of the
Polish Academy of Sciences

Content of presentation

1. Introduction
2. The aim of the work
3. Thermomechanical problem

   a) Taylor bar b) WC/Co plate

4. Brittle platelet impact, Al2O3/ZrO2
5. SiC foam fast compression
6. SiC foam impact
7. Summary

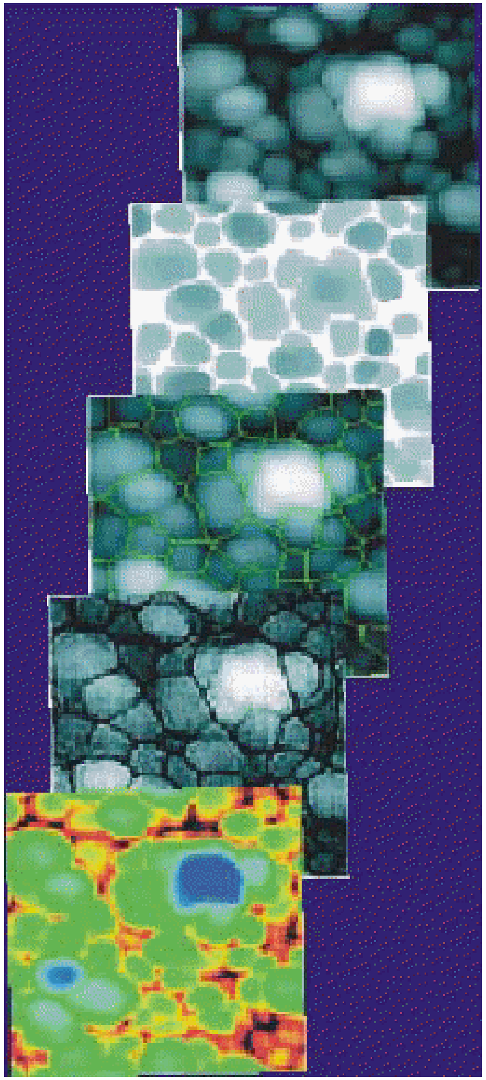

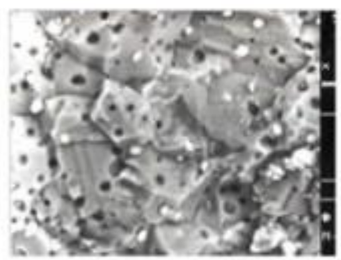

WC/Co

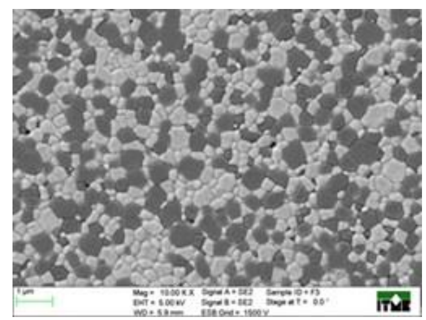

Al2O3/Zr02

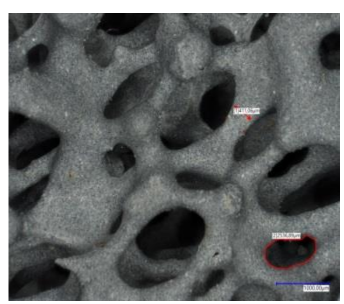

SiC

AlSi12/SiC

Problem statement

$$\mathbf{KT} + \mathbf{C}\dot{\mathbf{T}} = \mathbf{F}$$

Thermal equation of equilibrium, fulfills boundary and initial conditions

$\mathbf{T}, \quad \dot{\mathbf{T}}$ are the temperature vector and temperature rate vector

$\mathbf{K}$ is the conductivity matrix, $\mathbf{C}$ is the heat capacity matrix (diagonal), $\mathbf{F}$ is the vector of thermal source and fluxes

$$\mathbf{M}\ddot{\mathbf{u}} = \mathbf{f} - \mathbf{p}$$

$\mathbf{M}$ is the diagonal mass matrix, $\mathbf{u}$ is the displacement vector, $\ddot{\mathbf{u}}$ is the nodal acceleration vetor, $\mathbf{f}$ is the internal force vetor and $\mathbf{p}$ is the nodal load vector

$$\ddot{\mathbf{u}}_n = \left(\mathbf{M}\right)^{-1}\left(\mathbf{f}_n - \mathbf{p}_n\right)$$

where n denotes the current time step and Δt is the time interval

$$\dot{\mathbf{u}}_{n+1/2} = \mathbf{u}_{n-1/2} + \ddot{\mathbf{u}}_n \Delta t$$

Velocity; $\mathbf{u}_{n+1} = \mathbf{u}_n + \dot{\mathbf{u}}_{n+1/2} \Delta t$ displacements

$$\mathbf{T}_{n+1} = \left(\mathbf{C}\right)^{-1}\left(\mathbf{F}_n - \mathbf{K}_n \mathbf{T}_n\right)$$

Nodal temperature vector

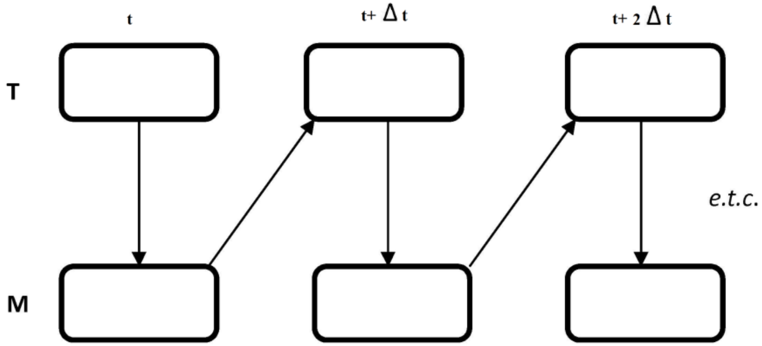

Staggered solution

$$f = \chi \boldsymbol{\sigma} : \mathbf{e}^{pl}$$

f is the heat flux due to plastic strain; $\boldsymbol{\sigma}$ is the Cauchy stress tensor, $\mathbf{e}$pl is the plastic strain deformation rate

$$\sigma^{o} = \left(A + B\left(\bar{\varepsilon}^{pl}\right)^{n}\right)\left(1 + C \ln \dot{\varepsilon}^{*}\right)\left(1 - \zeta^{m}\right)$$

A is the yield stress, B is the hardening coefficient, C is the strain rate coefficient, $\bar{\varepsilon}^{pl}$ is the equivalenet plastic strain, $\dot{\varepsilon}^{*}$ is the rate of the equivalent plastic strain

$$\zeta = \begin{cases} 0 & for \quad T < T_{trans} \\ \left(T - T_{trans}\right) / \left(T_{melt} - T_{trans}\right) & for \quad T_{trans} \le T \le T_{melt} \\ 1 & for \quad T > T_{melt} \end{cases}$$

where T is the current temperature, T_{trans} is the temperature around which the yield stress becomes temperature-dependent, and T_{melt} is the melting temperature.

Taylor bar

Parameters of the Johnson-Cook material model.

Parameters	Values and units
Young's modulus	2.1×10^5 MPa
Poisson's coefficient	0.296
Yield stress (A)	455.0 MPa
Hardening coefficient (B)	2475.0 MPa
Hardening exponent (n)	0.9
Strain rate coefficient C	0.0235
Thermal softening exponent (m)	1.0
Melt temperature T_{melt}	1728 K
Transition temperature T_{trans}	293 K
Specific heat C_H	440 J/kg K
Thermal conductivity K	150 W/m K
Thermal expansion α_t	5.0×10^{-5} 1/K
Mass density	9130 kg/m^3

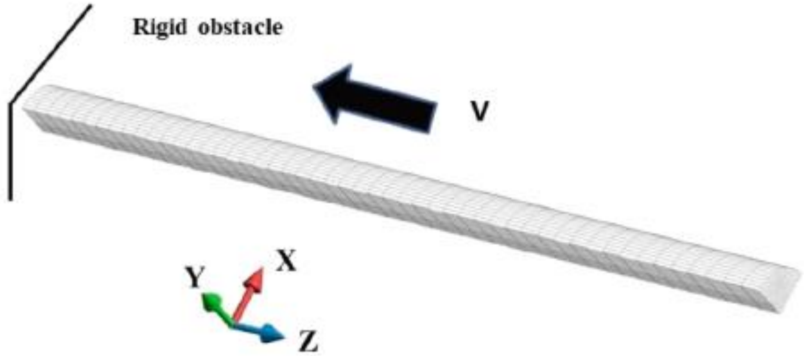

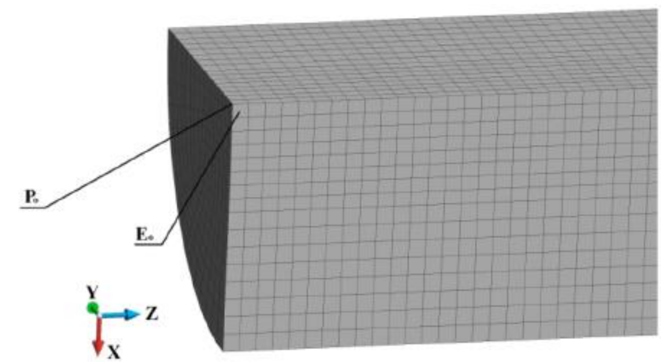

Maximum displacement, equivalent plastic strain, temperature in analyzed meshing cases, and a comparison between the adiabatic and coupled solutions.

Case		Number of nodes and elements	Displacement $\times 10^{-2}$ m	Equivalent plastic strain (Element *Eo*)	Temperature, [K] (Element *Eo*)	Equivalent plastic strain (Node *Po*)	Temperature, [K] (Node *Po*)
B1	Adiabatic	Nds 21,917	1.068	1.206	759.4	1.156	759.3
	Coupled	Els 19,200	1.072	1.203	707.6	1.154	707.6
B2	Adiabatic	Nds 32,767	1.068	1.195	780.4	1.195	780.3
	Coupled	Els 28,800	1.070	1.193	720.3	1.193	720.3
B3	Adiabatic	Nds 43,617	1.067	1.206	786.2	1.206	786.2
	Coupled	Els 38,400	1.071	1.203	724.3	1.203	724.3
B4	Adiabatic	Nds 54,467	1.069	1.210	788.0	1.210	788.0
	Coupled	Els 48,000	1.071	1.206	725.7	1.206	725.6

Adiabatic solution

Coupled solution

(c)

(d)

Impact velocity 350 m/s

Eq plastic strain

Temperature

Adiabatic solution

Coupled solution

Impact velocity 550 m/s

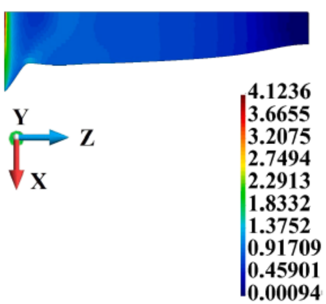

(c)

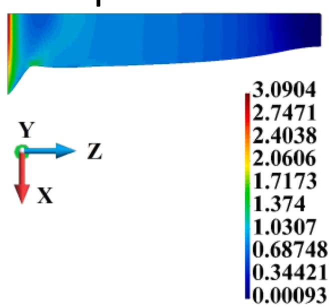

(d)

Eq plastic strain

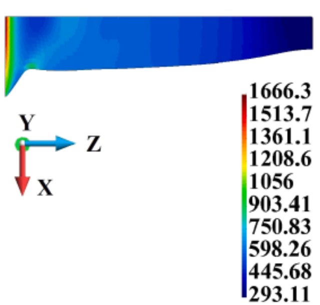

(e)

Temperature

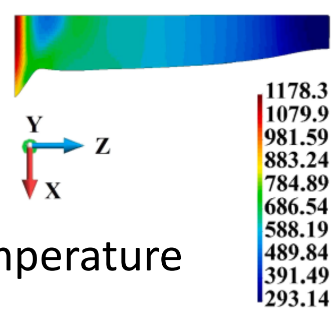

(f)

	Displacement $\times 10^{-2}$ m	Equivalent plastic strain (element Eo)
Adiabatic	1.742	4.124
Coupled	1.740	3.090

Temperature [K] (Element Eo)	Equivalent plastic strain (Node Po)
1666.3	4.134
1178.3	3.092

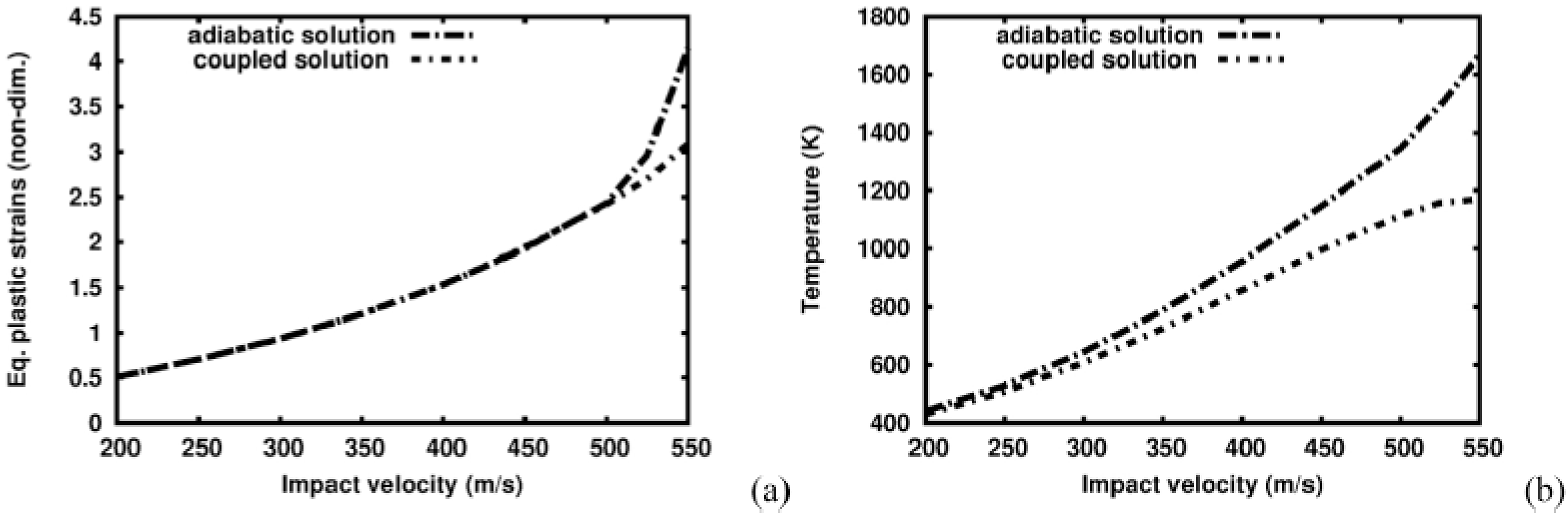

Relationship between the maximum equivalent plastic strain (a) and the maximum temperature (b) and the impact velocity in the adiabatic and coupled solutions.

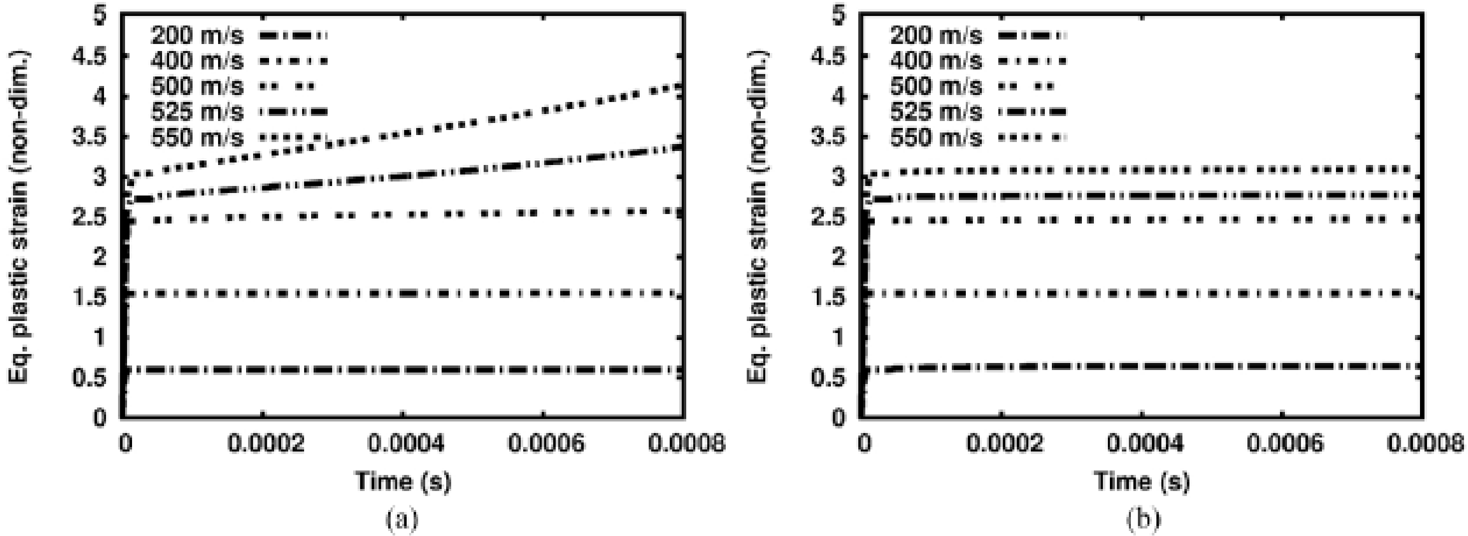

Time variation of the maximum equivalent plastic strain for different impact velocities; (a) adiabatic solution, (b) coupled solution

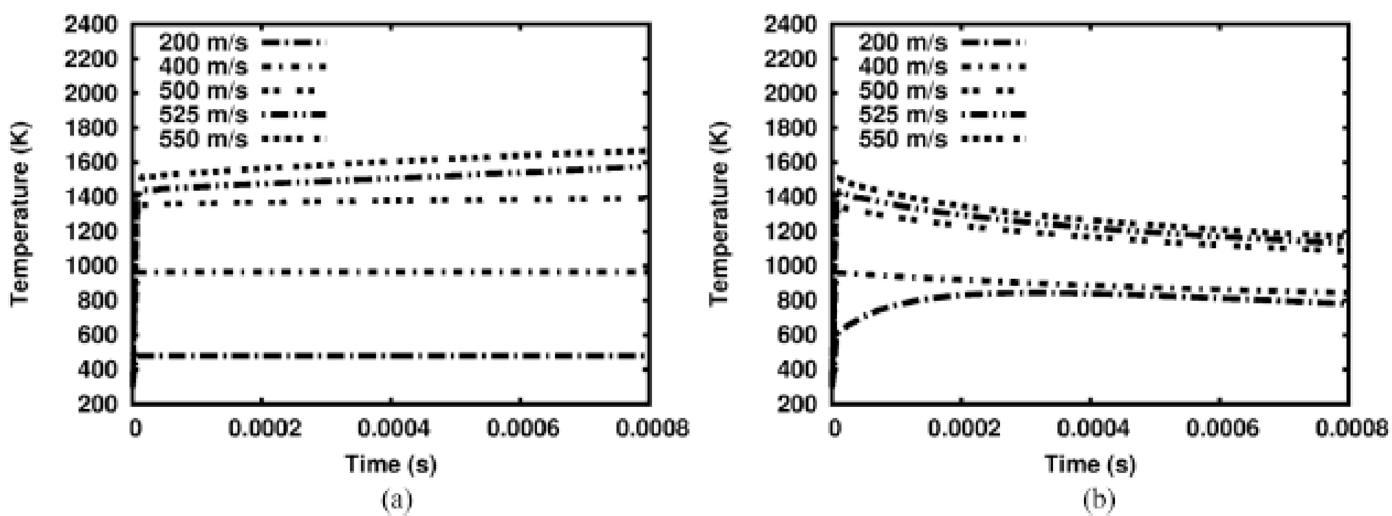

Time variation of the maximum temperature for different impact velocities; (a) adiabatic solution, (b) coupled solution.

WC/Co composite model

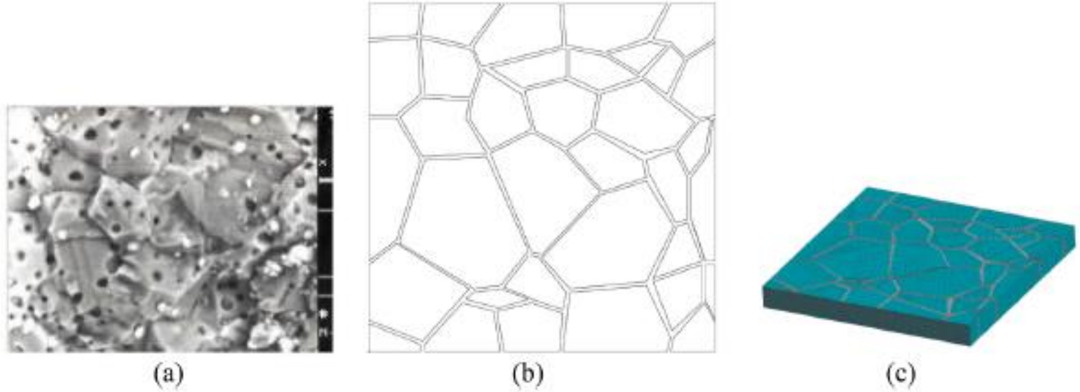

Parameters	Values and units
Young's modulus	6.2×10^5 MPa
Poisson's coefficient	0.215
Specific heat C_H	250 J/kg K
Thermal conductivity K	95 W/m K
Thermal expansion α_t	1.5×10^{-5} 1/K
Mass density	14,770 kg/m^3

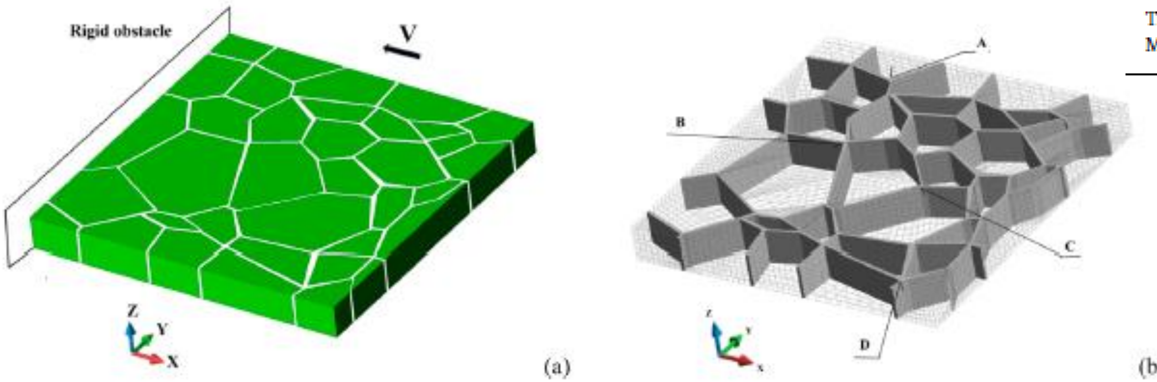

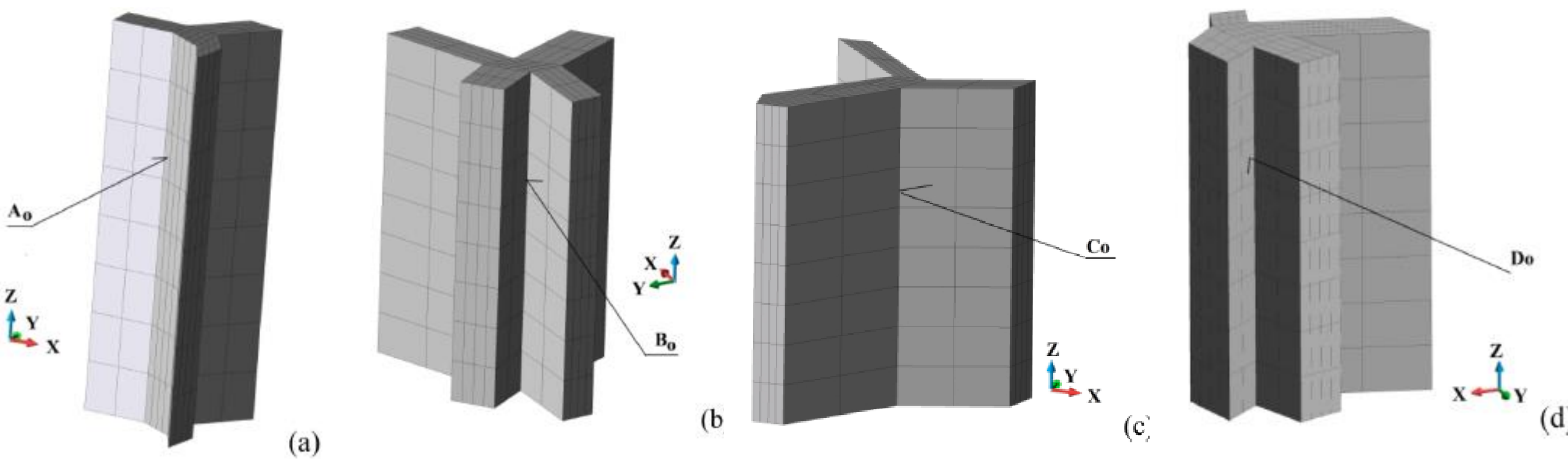

Junctions A, B, C and D

Mesh dependency check

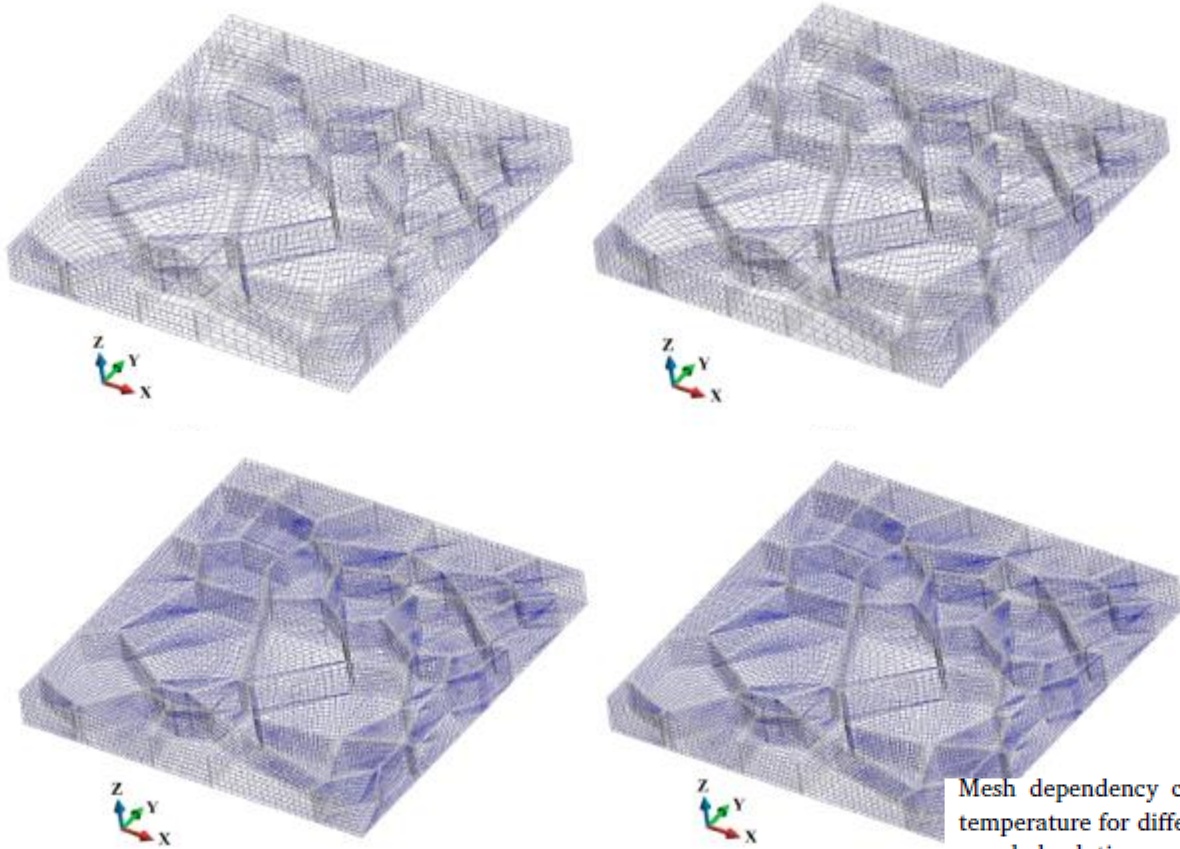

(c) (d)

Mesh dependency check. Maximum displacement, equivalent plastic strain, temperature for different meshes, and a comparison between the adiabatic and coupled solutions.

Case		Number of nodes and elements	Displacement x 10^{-6} m	Equivalent plastic strain	Temperature [K]
P1	Adiabatic	Nds 40,726/	1.7353	3.6238	1646.7
	Coupled	Els 15,516/ 18,666	1.3320	2.0727	386.7
P2	Adiabatic	Nds 75,634/	1.6199	3.5469	1637.9
	Coupled	Els 31,032/ 37,332	1.2579	2.0431	385.7
P3	Adiabatic	Nds 101,486/	1.7254	3.5429	1637.3
	Coupled	Els 24,252/ 61,554	1.3419	2.1045	389.6
P4	Adiabatic	Nds 130,482	1.6259	3.5189	1634.4
	Coupled	Els 32,336/ 82,072	1.2776	2.0772	389.0

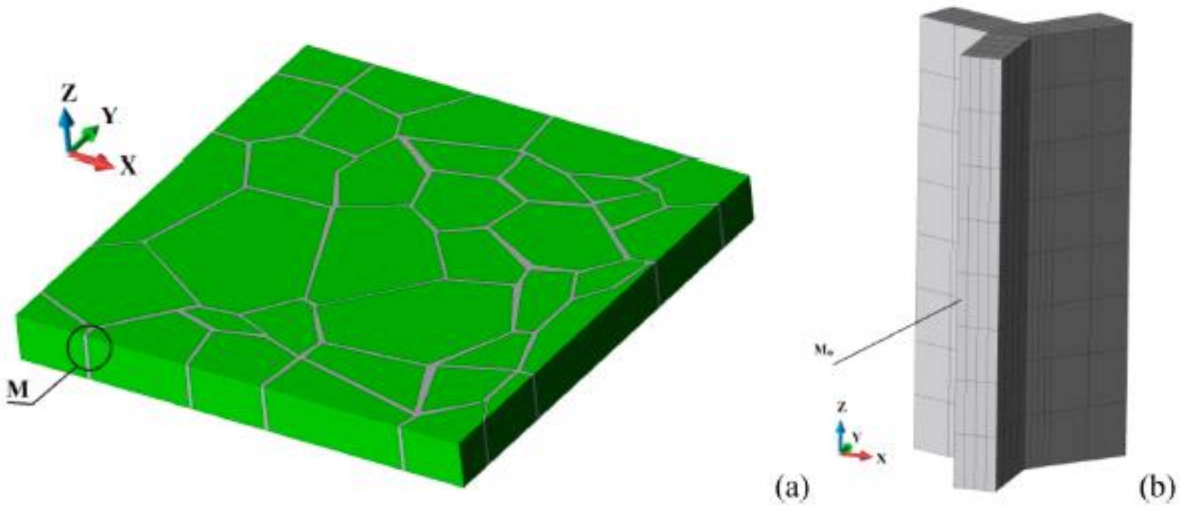

(a) region of the maximum equivalent plastic strain and temperature, (b) detail of the mesh with Element Mo

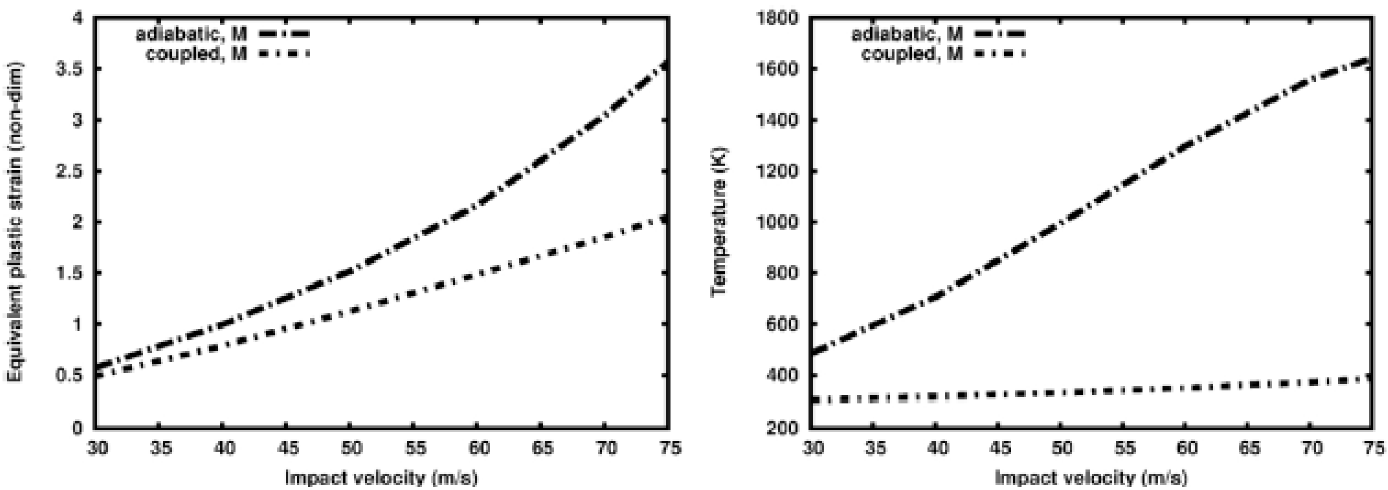

Comparison of the adiabatic and coupled solutions depending on the impact velocity at Element Mo; (a) equivalent plastic strain, (b) temperature

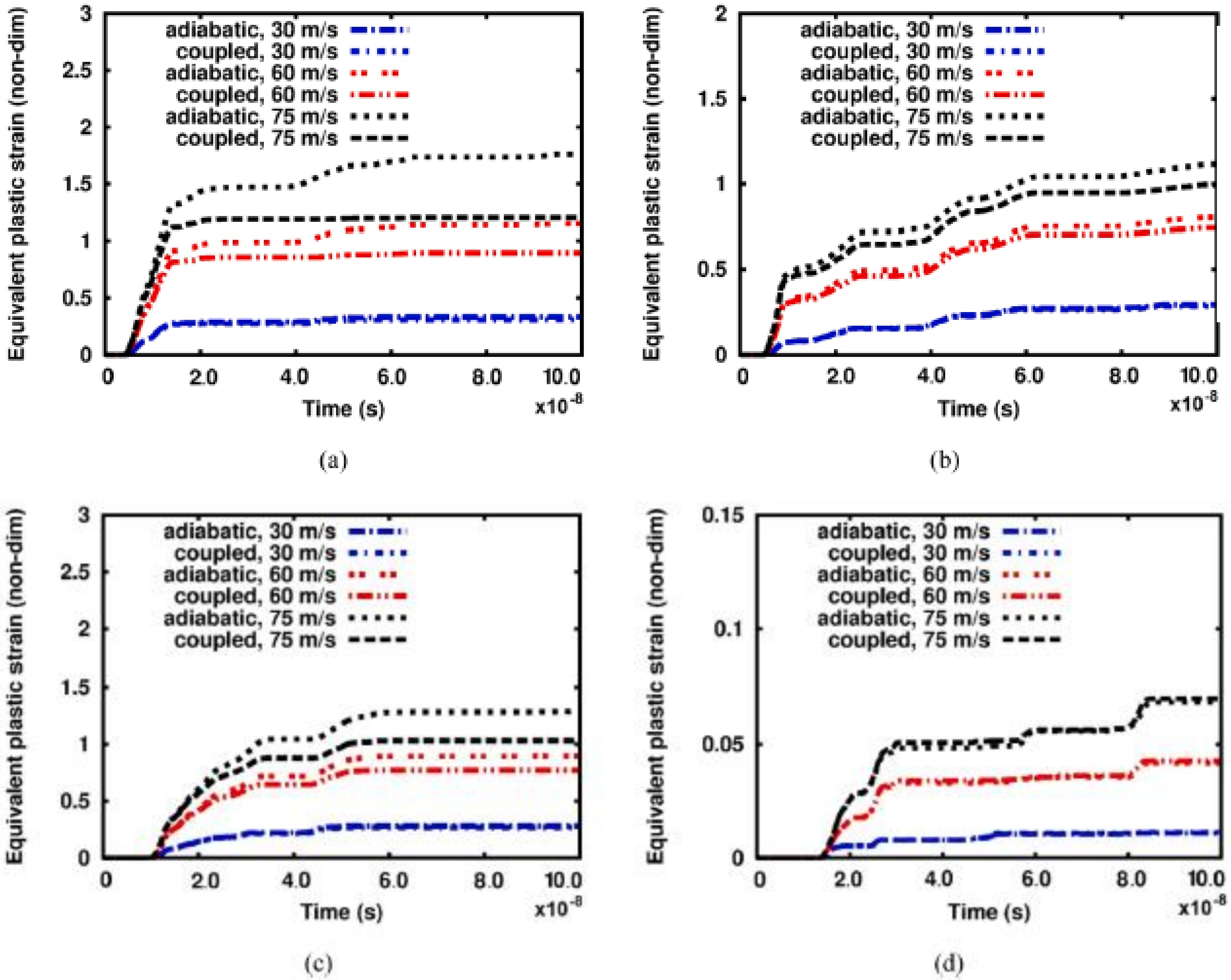

	Equivalent plastic strain								
Velocity	30 m/s			60 m/s			75 m/s		
Junction	Adiabatic	Coupled	%	Adiabatic	Coupled	%	Adiabatic	Coupled	%
A	0.331	0.309	7.2	1.151	0.897	22.1	1.762	1.205	31.6
B	0.293	0.285	2.7	0.805	0.742	7.8	1.117	0.995	10.9
C	0.283	0.268	5.8	0.897	0.773	13.8	1.292	1.033	20.0
D	0.011	0.011	0.0	0.042	0.042	0.0	0.069	0.070	1.4

Equivalent plastic strain in the adiabatic an coupled solutions; (a) Junction A, (b) Junction B, (c) Junction C, (d) Junction D.

Impact velocity versus equivalent plastic strain at Junctions A, B, C and D towards the end of the process.

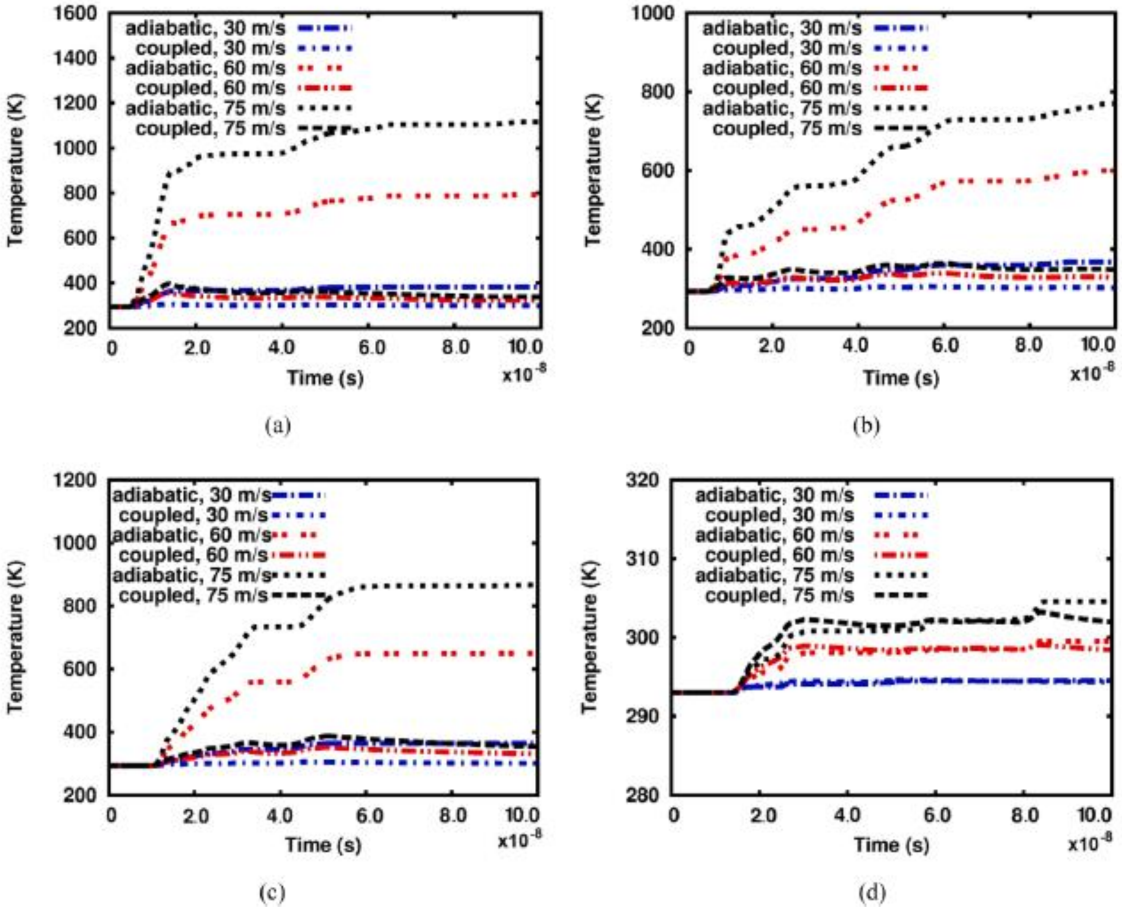

Temperature in the adiabatic and coupled solutions; (a) Junction A, (b) Junction B, (c) Junction C, (d) Junction D.

Velocity	Temperature 30 m/s			60 m/s			75 m/s		
Junction	Adiabatic	Coupled	%	Adiabatic	Coupled	%	Adiabatic	Coupled	%
A	382	300	21.5	793	322	59.4	1116	338	230.2
B	367	302	17.2	600	328	45.3	770	245	214.3
C	364	301	17.3	650	331	49.1	868	354	145.2
D	294	294	0.0	300	298	0.7	305	302	1.0

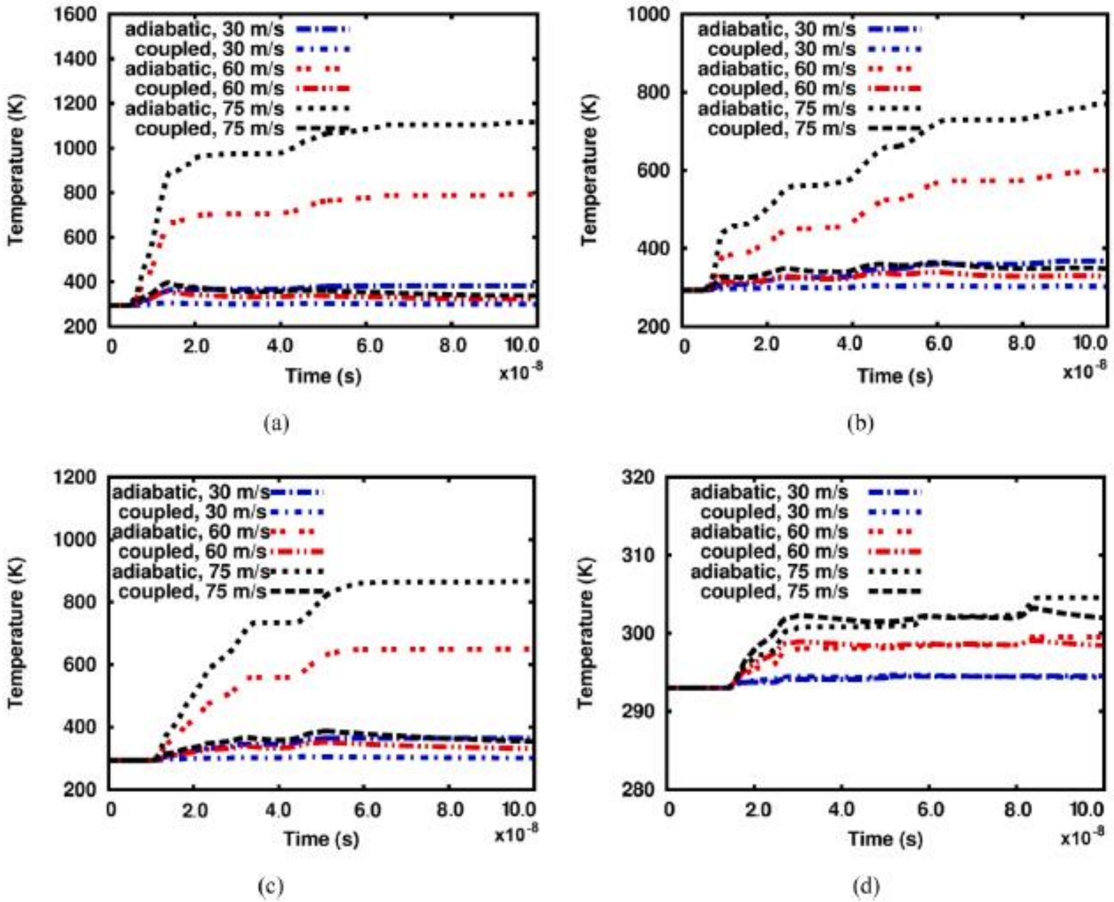

Temperature in the adiabatic and coupled solutions; (a) Junction A, (b) Junction B, (c) Junction C, (d) Junction D.

	Temperature								
Velocity	30 m/s			60 m/s			75 m/s		
Junction	Adiabatic	Coupled	%	Adiabatic	Coupled	%	Adiabatic	Coupled	%
A	382	300	21.5	793	322	59.4	1116	338	230.2
B	367	302	17.2	600	328	45.3	770	245	214.3
C	364	301	17.3	650	331	49.1	868	354	145.2
D	294	294	0.0	300	298	0.7	305	302	1.0

Temperature at the end of the process

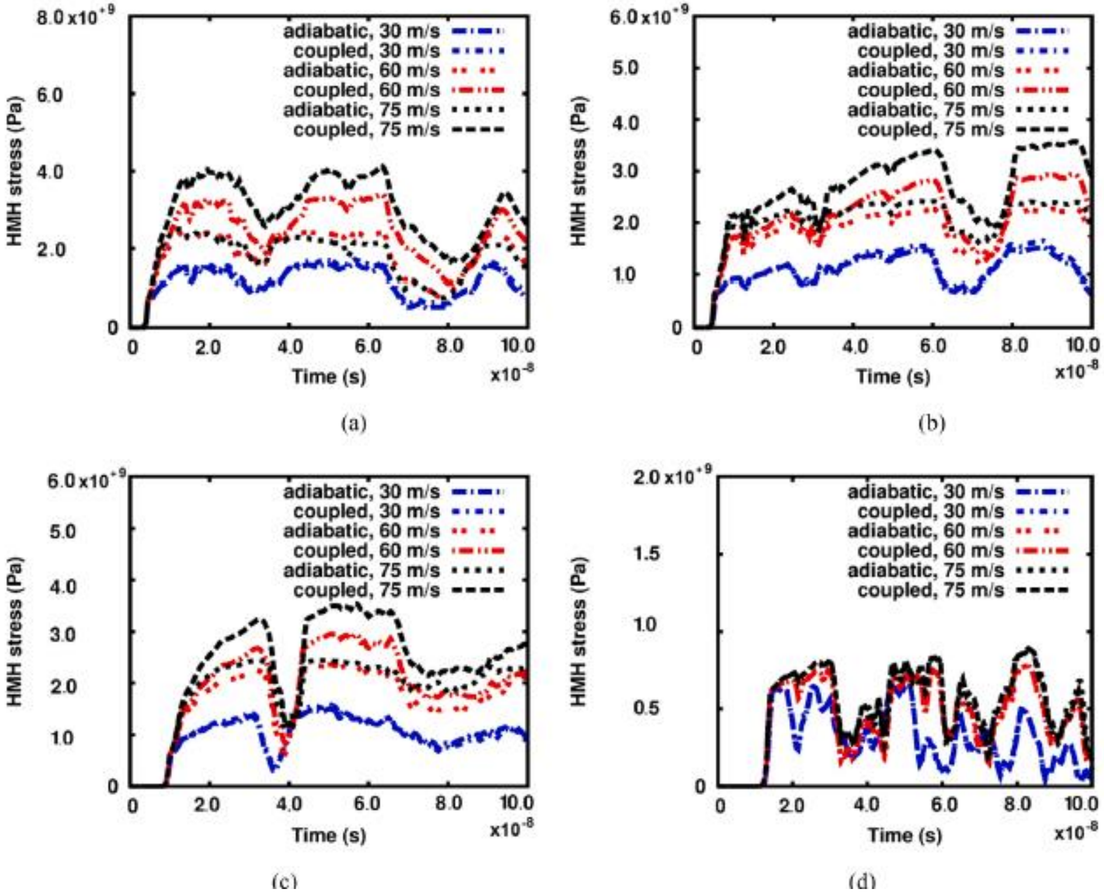

HMH stress in the adiabatic and coupled solutions; (a) Junction A, (b) Junction B, (c) Junction C, (d) Junction D.

HMH stress versus impact velocity at Junctions A, B, C and D, time instant: 6.0×10^{-8} s.

	HMH stress								
Velocity	30 m/s			60 m/s			75 m/s		
Junction	Adiabatic $\times 10^{+9}$	Coupled $\times 10^{+9}$	%	Adiabatic $\times 10^{+9}$	Coupled $\times 10^{+9}$	%	Adiabatic $\times 10^{+9}$	Coupled $\times 10^{+9}$	%
A	1.465	1.537	4.9	2.341	3.294	40.7	2.087	3.891	86.4
B	1.333	1.291	3.2	2.256	2.827	25.3	2.413	3.407	47.2
C	1.271	1.264	0.6	2.138	2.684	25.5	2.283	3.292	44.2
D	0.102	0.116	13.7	0.488	0.487	0.20	0.638	0.635	0.5

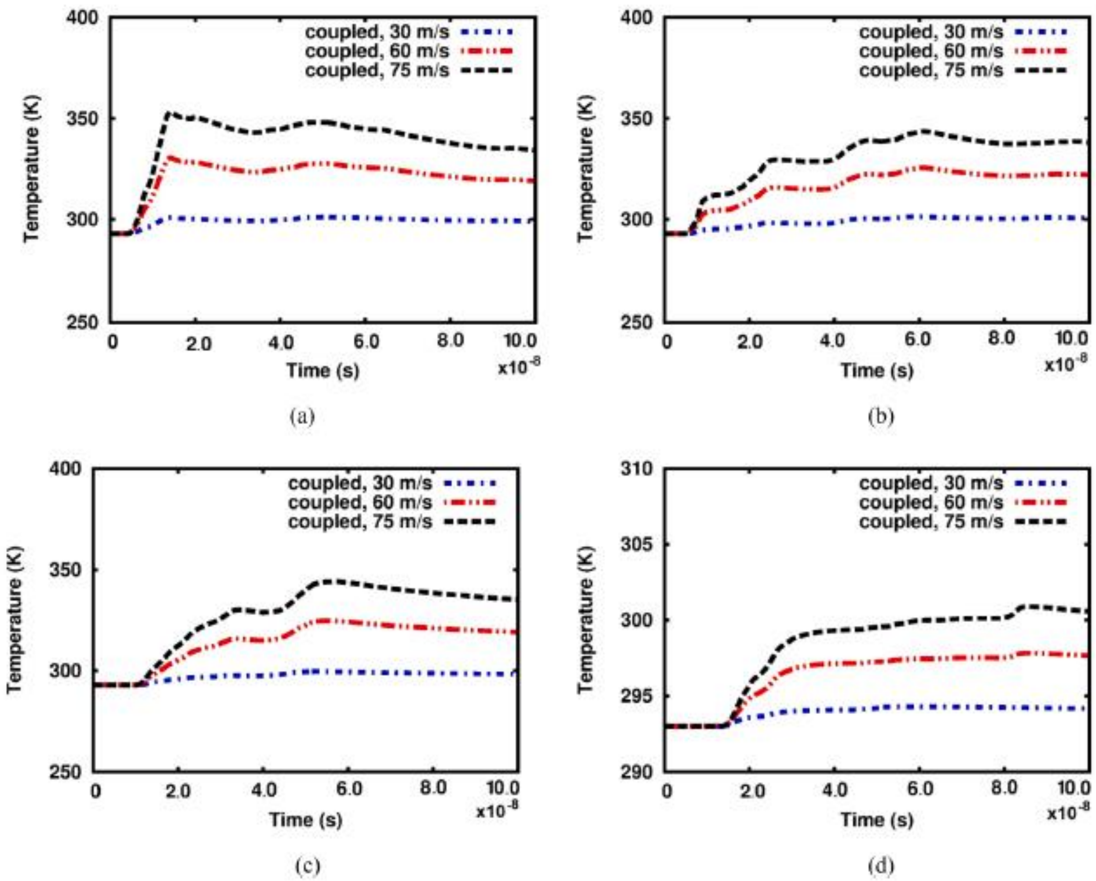

Temperature at Elements Aa, Ba, Ca and Da in the grains adjacent to the binders, coupled solution; (a) Junction A, (b) Junction B, (c) Junction C, (d) Junction D.

	Temperature		
Velocity	30 m/s	60 m/s	75 m/s
Element adjacent to Junction	[K]	[K]	[K]
A	301	326	344
B	301	325	344
C	299	324	343
D	294	297	300

Impact velocity versus temperature in the grains at Elements Aa, Ba, Ca and Da adjacent to Junctions A, B, C and D, time instant: 6.0 × 10−8 s.

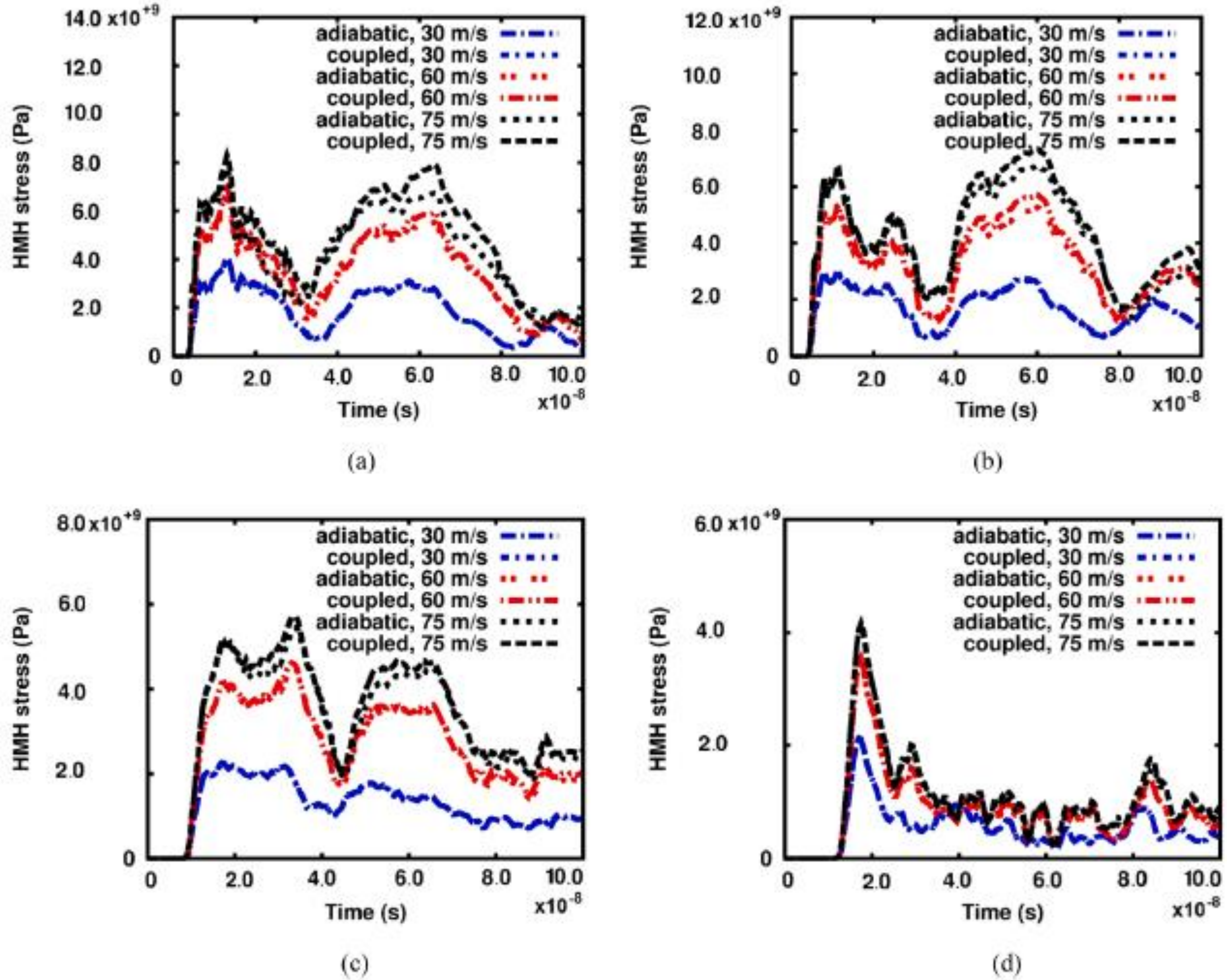

HMH stress at Elements Aa, Ba, Ca and Da in the grains adjacent to the binders in the adiabatic and coupled solutions; (a) Junction A, (b) Junction B, (c)
Junction C, (d) Junction D.

	HMH stress								
Velocity	30 m/s			60 m/s			75 m/s		
Junction	Adiabatic $\times 10^{+9}$	Coupled $\times 10^{+9}$	%	Adiabatic $\times 10^{+9}$	Coupled $\times 10^{+9}$	%	Adiabatic $\times 10^{+9}$	Coupled $\times 10^{+9}$	%
A	2.803	2.837	1.2	5.371	5.779	32.2	6.526	7.525	15.3
B	2.076	2.631	27	5.260	5.772	9.7	6.752	7.329	7.2
C	1.429	1.416	1.0	3.378	3.430	1.5	4.286	4.443	3.7
D	0.279	0.309	11.0	0.691	0.664	3.9	0.840	0.828	1.4

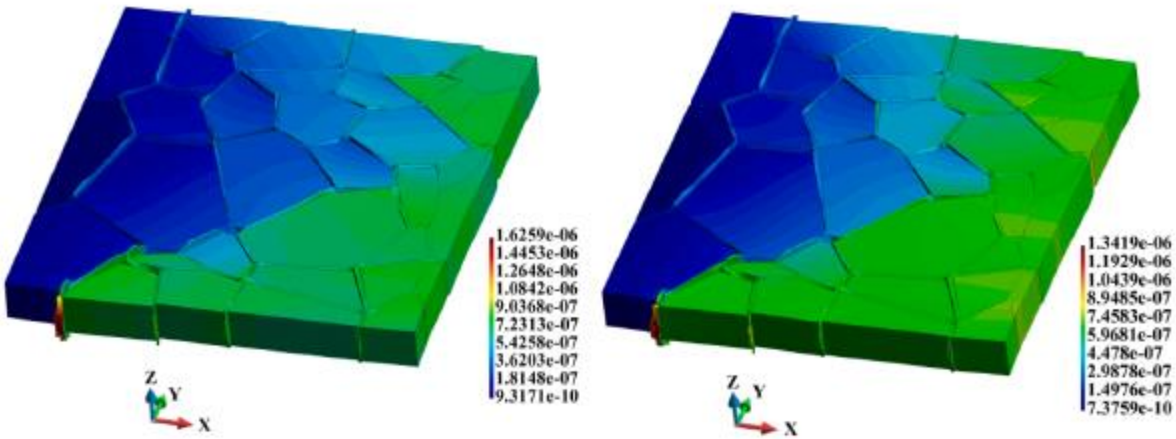

Displacement (m) fields (magnified 5 times); (a) adiabatic solution; (b) coupled solution.

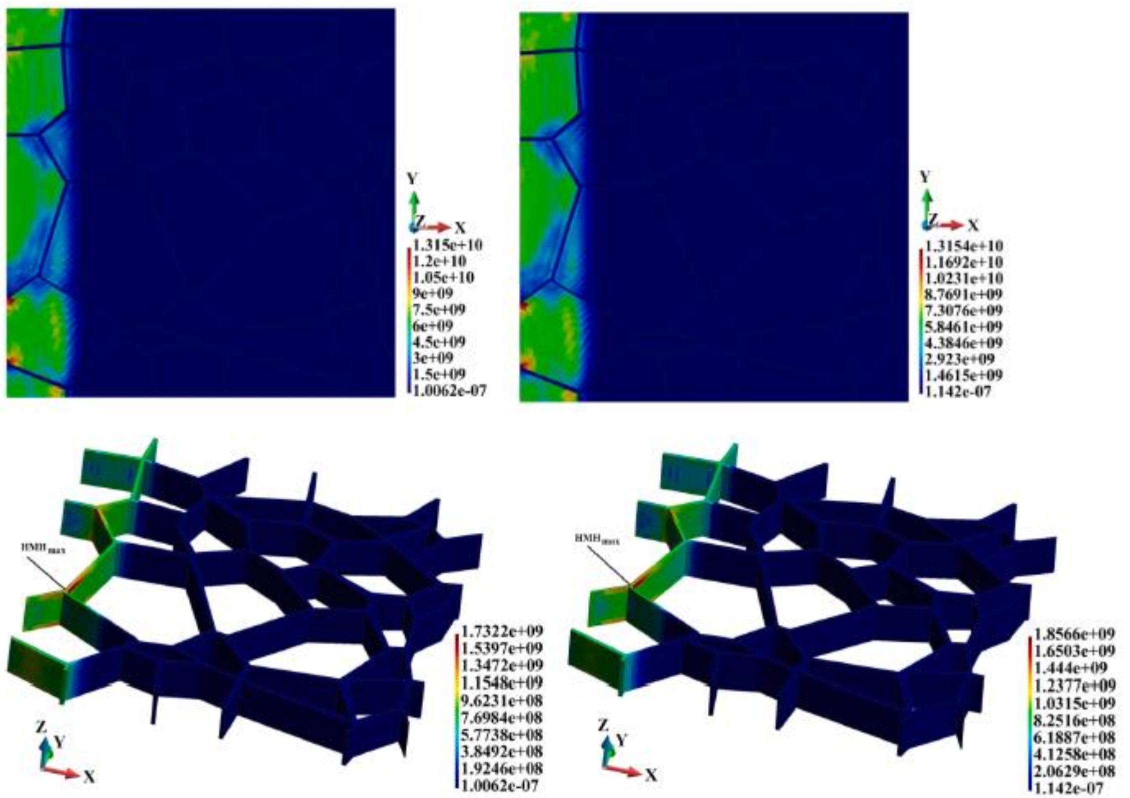

HMH stress (Pa), time instant: 2.5 × 10−9 s; (a) adiabatic solution, (b) coupled solution.

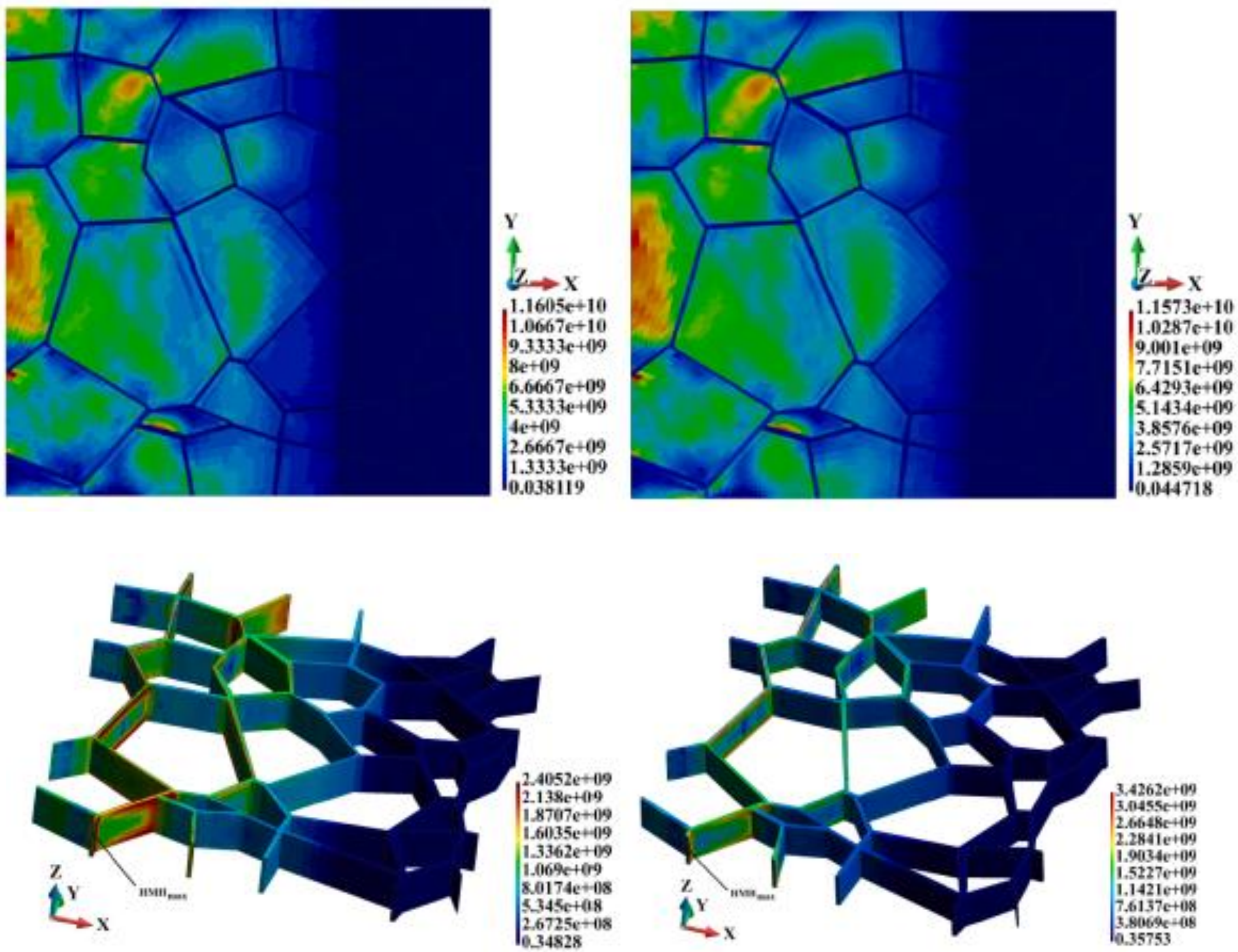

HMH stress (Pa) in the binders, time instant: 10.0 × 10−9 s;
(a) adiabatic solution, (b) coupled solution.

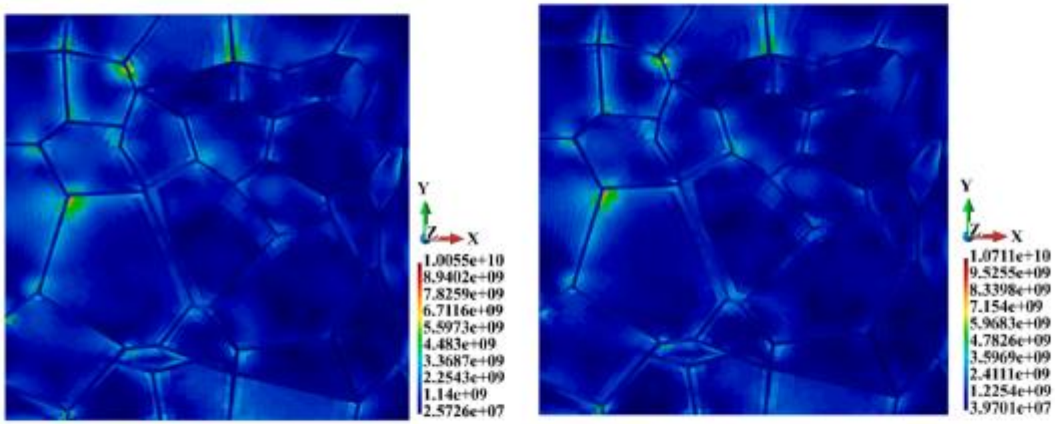

HMH stress (Pa), time instant: 75.0 × 10−9 s; (a) adiabatic solution, (b) coupled solution.

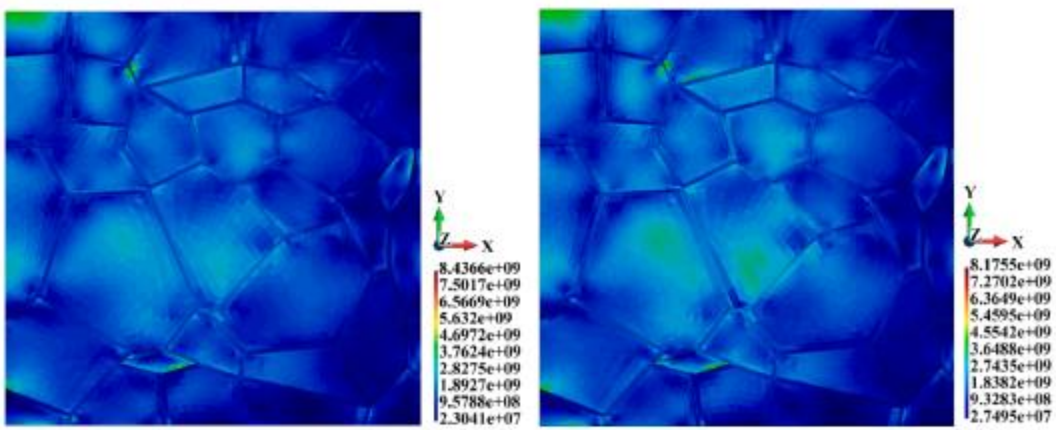

HMH stress (Pa), time instant: 100 × 10−9 s; (a) adiabatic solution; (b) coupled solution.

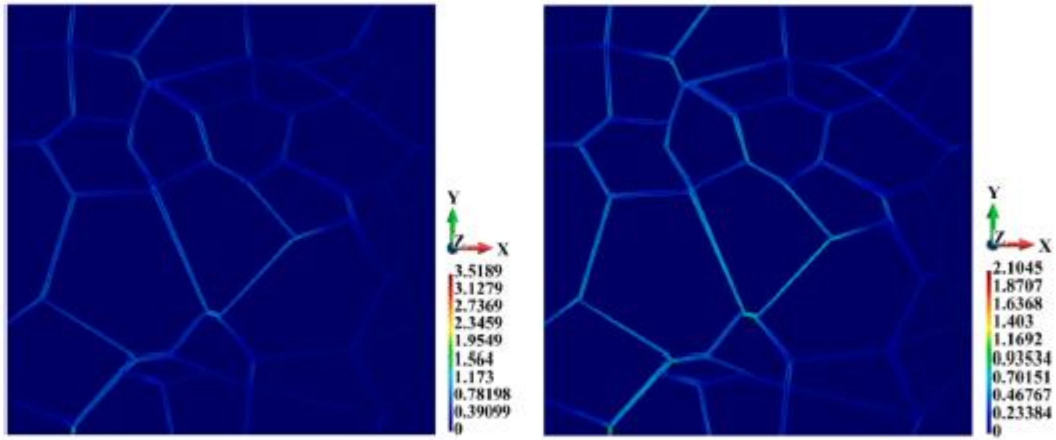

Equivalent plastic strain variations at the junctions; (a) adiabatic solution; (b) coupled solution; impact velocity 75 m/s

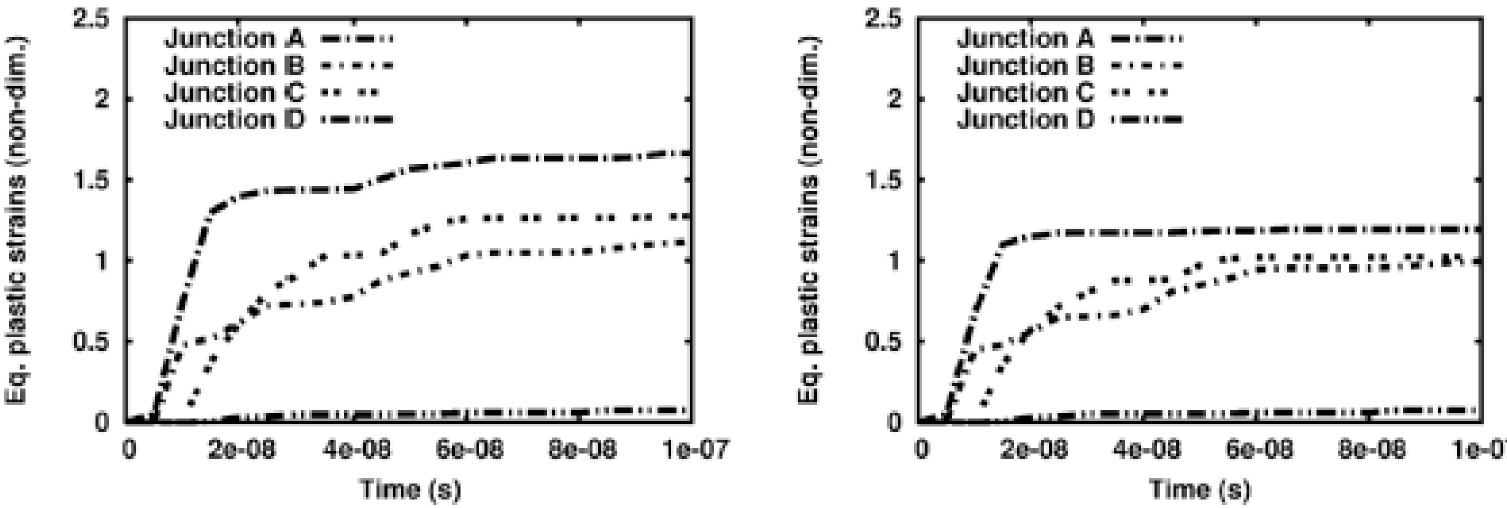

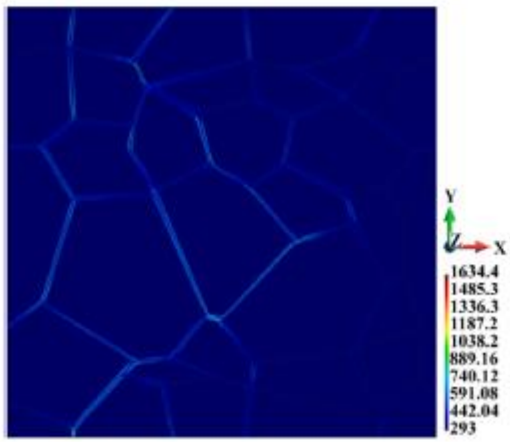

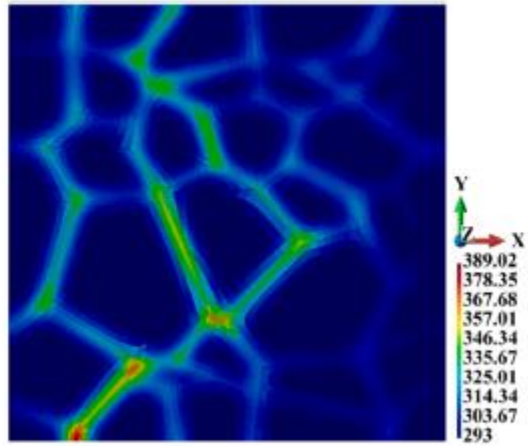

Temperature distribution (K); (a) adiabatic solution; (b) coupled solution`, End of the process, Impact velocity 75 m/s

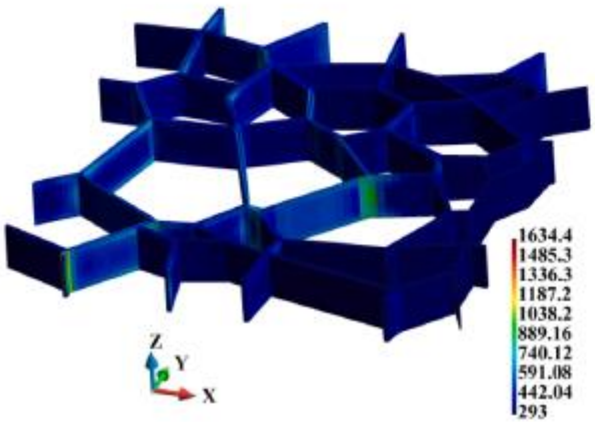

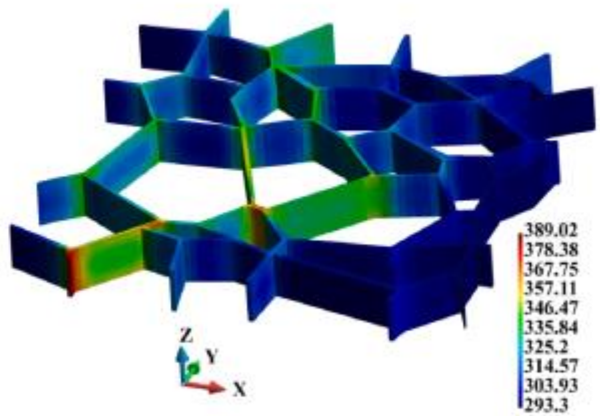

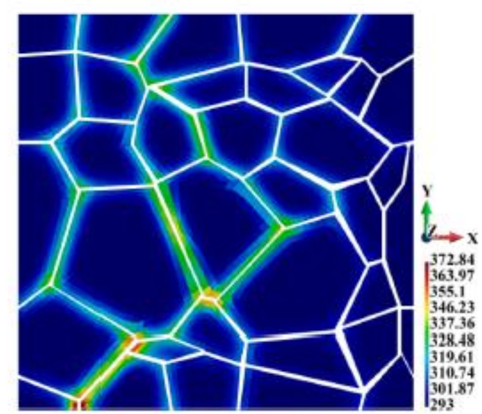

- The displacement fields obtained for the two solutions are qualitatively similar;
- Although the HMH stress fields in both cases are similar with respect to quality, the maximum stress in the binders is lower than that in the grains;
- The equivalent plastic strains in the binders are lower in the coupled solution;
- The maximum temperature is significantly lower in the coupled solution;
- The polycrystalline material grains are affected by temperature increase;
- Given the significant differences in the solutions, the adiabatic solution should not be used for the analysis of polycrystalline materials.

Peridynamics method

Q and **x** are the points inside an undeformed body. The bond definition

$$\boldsymbol{\xi} = \mathbf{Q} - \mathbf{x}$$

The reference state **X** is a function that is valid on the bond **X(ξ)**. The deformation state is dependent on the new position of the coordinate **x** in the deformed body **y(x)** in the following way

$$\mathbf{Y}(\mathbf{x}, \boldsymbol{\xi}) = \mathbf{y}(\mathbf{x} + \boldsymbol{\xi}) - \mathbf{y}(\mathbf{x}),$$

$$\mathbf{Y}(\mathbf{x}, \boldsymbol{\xi}) = \mathbf{y}(\mathbf{Q}) - \mathbf{y}(\mathbf{x}).$$

The state of displacements is:

$$\mathbf{U}(\mathbf{x}, \boldsymbol{\xi}) = \mathbf{u}(\mathbf{x} + \boldsymbol{\xi}) - \mathbf{u}(\boldsymbol{\xi}),$$

$$\mathbf{U}(x, \xi) = \mathbf{u}(Q) - \mathbf{u}(x).$$

The scalar extension state e(**Y**) is of the form:

$$e(\mathbf{Y}) = |\mathbf{Y}| - |\mathbf{X}|.$$

The decomposition of the scalar extension state into spherical and deviatoric components

$$e = e^i + e^d.$$

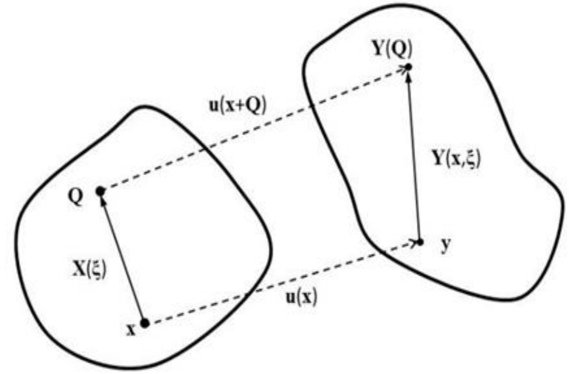

The force state t(**Y**) is shown in a form similar to the standard stress-strain relation that is the sum of its spherical and deviatoric parts

$$t(\mathbf{Y}) = \left(\frac{3k\theta}{m}\right)\omega x + \alpha\omega e^d.$$

k is the bulk modulus, θ is the dilatation, m is the weighted volume, ω is the influence function, $x = |\xi|$ is the basic scalar state, α = (15μ)/m is the coefficient being in relation to the shear modulus μ.

Peridynamics method

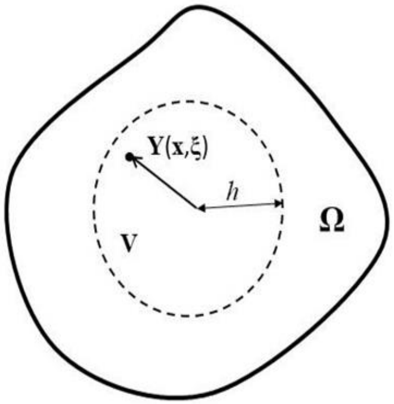

Integration scheme

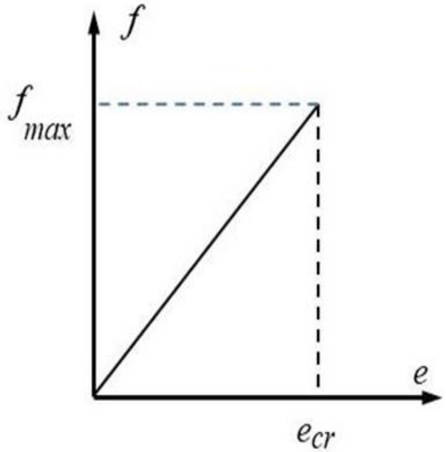

Constitutive law

The material failure model is based on the following assumptions: the bonds fail when their elongation overcomes the critical elongation; the total damage is due to the accumulation of broken bonds; and the bond breaking is an irreversible process.

The damage definion *d* reads:

$$d(x,t) = 1 - \frac{\int_{\Omega} \varsigma(x,t,\xi)\, d\Omega}{\int_{\Omega} d\Omega}.$$

The damage variable varies between 0 and 1. The value 0 means that the material is pristine while 1 means that the material is completely damaged.

A special case of the state-based model is the bond-based model

$$f = ce\varsigma(\mathbf{x}, t, \xi), \qquad c = (18k)/(\pi h^4)$$

c depends on the bulk modulus *k* and the horizon *h*

The failure is predominantly assumed on cracks appearance, the e_{cr} evaluation is based on fracture energy evaluation,

$$e_{cr} = \sqrt{\frac{5G_{ci}}{9kh}}$$

where G_{ci} is the fracture energy depending on the mode of failure

$$G_I = \frac{(1-\nu^2)K_I}{2E}$$

Contact

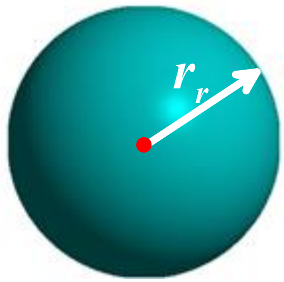

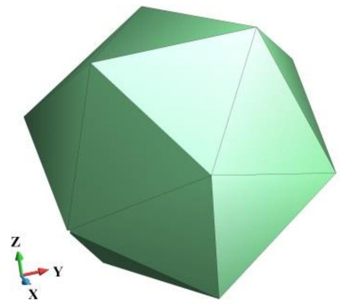

The contact is checked between the triangular facets of the bodies that are contact candidates.
The sphere is transformed into an icosahedron

Transformation of a sphere into an inscribed icosahedron: (**a**) sphere; (**b**) icosahedron.

$$f_{ct} = \begin{cases} C_t\left(r_r - d\right)V_1V_2 & for\, d \leq r_r \\ 0 & d > r_r \end{cases}$$

where d is the distance between the bodies, V_1 and V_2 are the volumes associated with the corresponding calculation points and C_t=18K_s/πh^5. The constant *Ks* is the artificial spring stiffness assumed as a high **penalty number** of the range 1.0E+12÷1.0E+20.

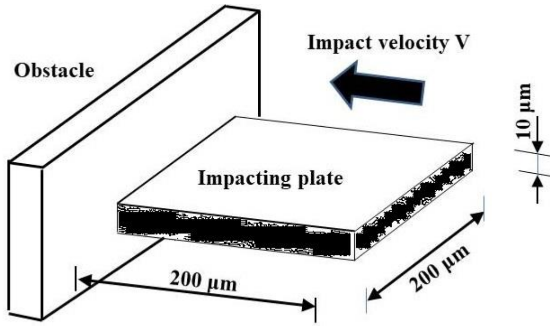

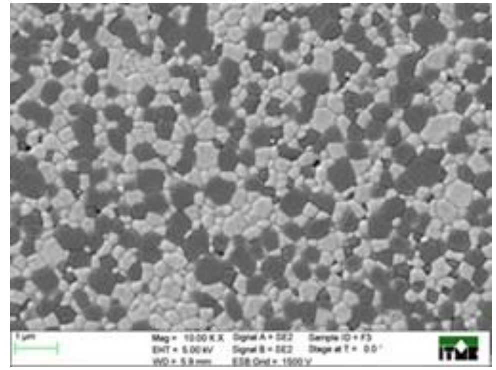

Al2O3/ZrO2

	Al_2O_3	ZrO_2
Young's modulus (GPa)	413	110
Poisson's ratio	0.21	0.22
Mass density (kg/m^3)	3980	5000
Maximum tensile stress (GPa)	665	115
Crushing strain	1.610E-03	9.563E-04

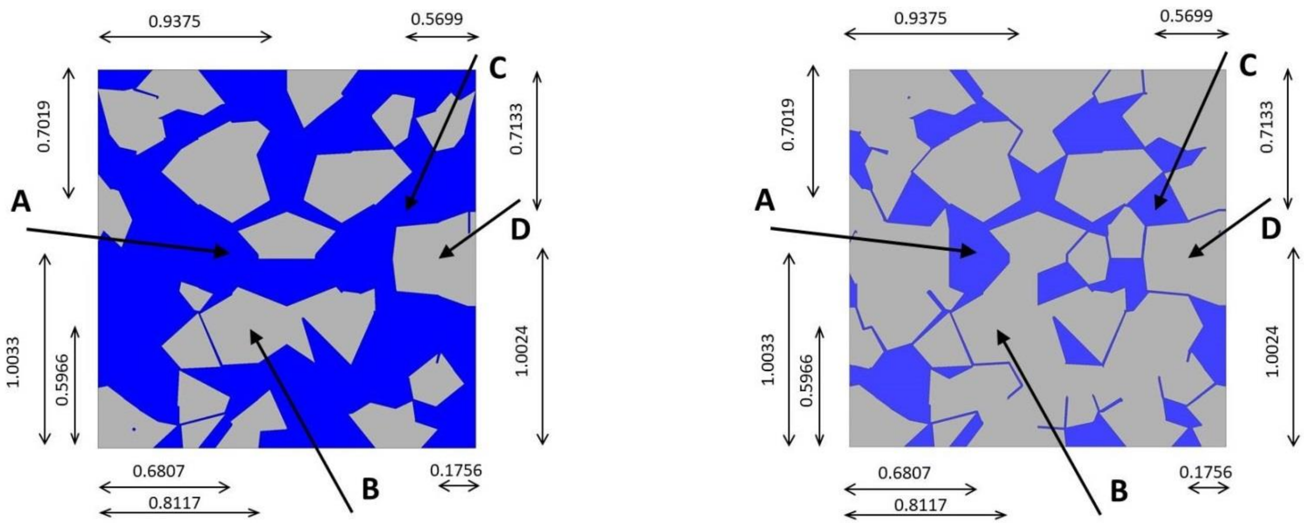

Schemes of the analyzed samples (dimension x1.0E-07 m), Al_2O_3 – grey, ZrO_2 - blue: (**a**) Low content of Al_2O_3, Case A (41%); (**b**) High content of Al_2O_3, Case B (75%).

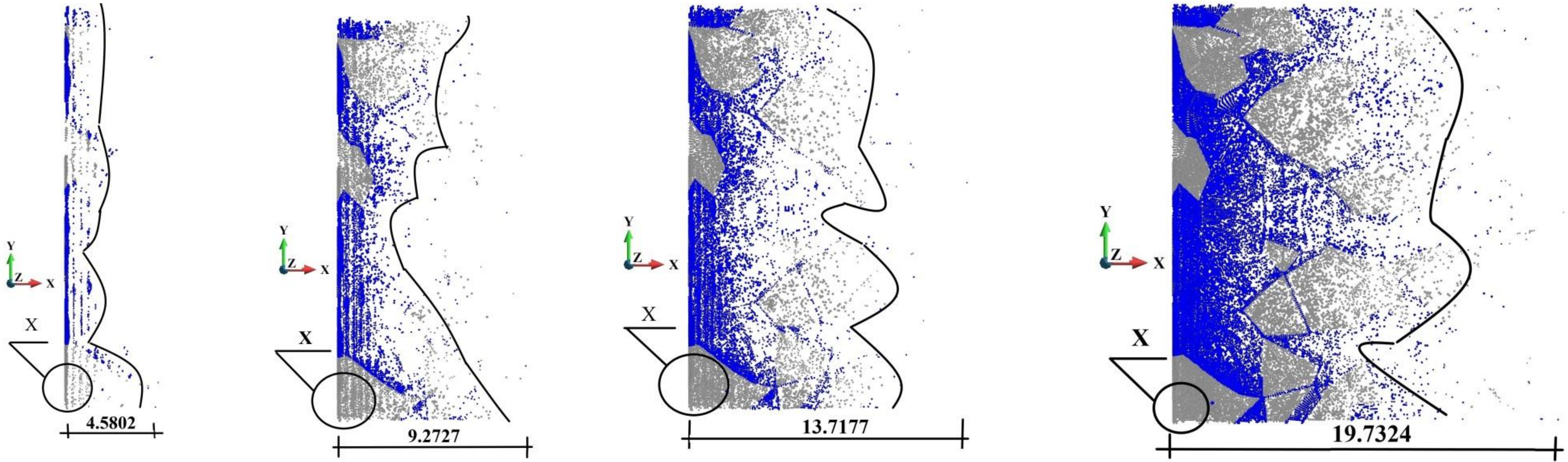

Damage advancement (dimension x 1.0E-5 m), Case A, impact velocity 60 m/s: (**a**) time 1.125E-08 s; (**b**) time 2.375E-08 s; (c) time 3.000E-07 s; (d) time 4.000E-08 s.

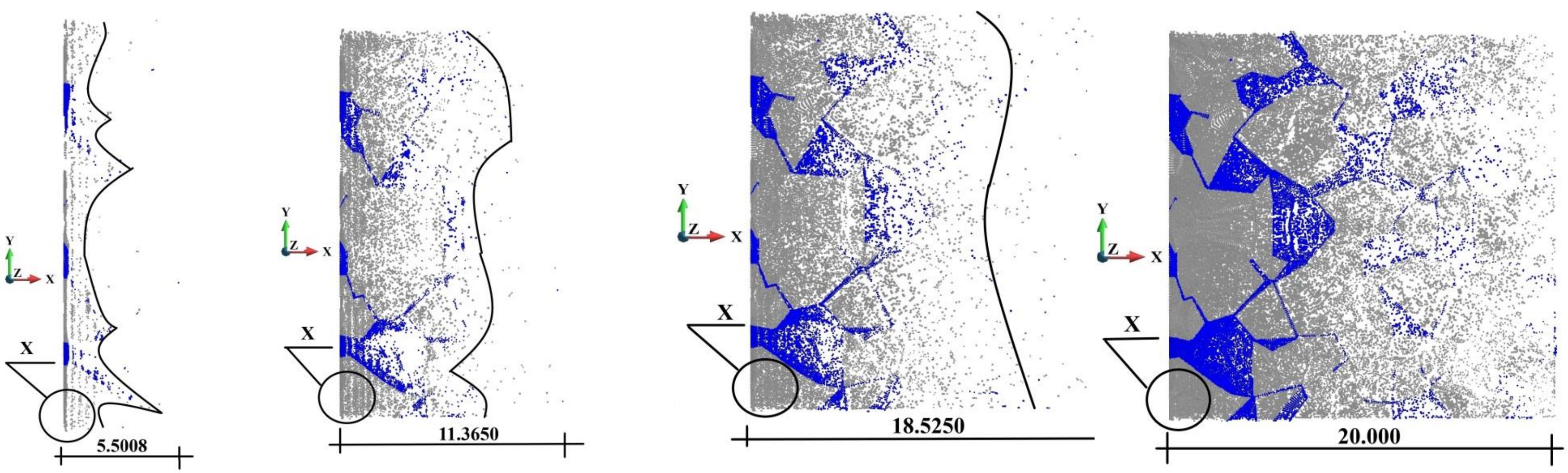

Damage advancement (dimension x 1.0E-5 m), Case B, impact velocity 60 m/s: (**a**) time 1.125E-08 s; (**b**) time 2.375E-08 s; (c) time 3.000E-07 s; (d) time 4.000E-08 s.

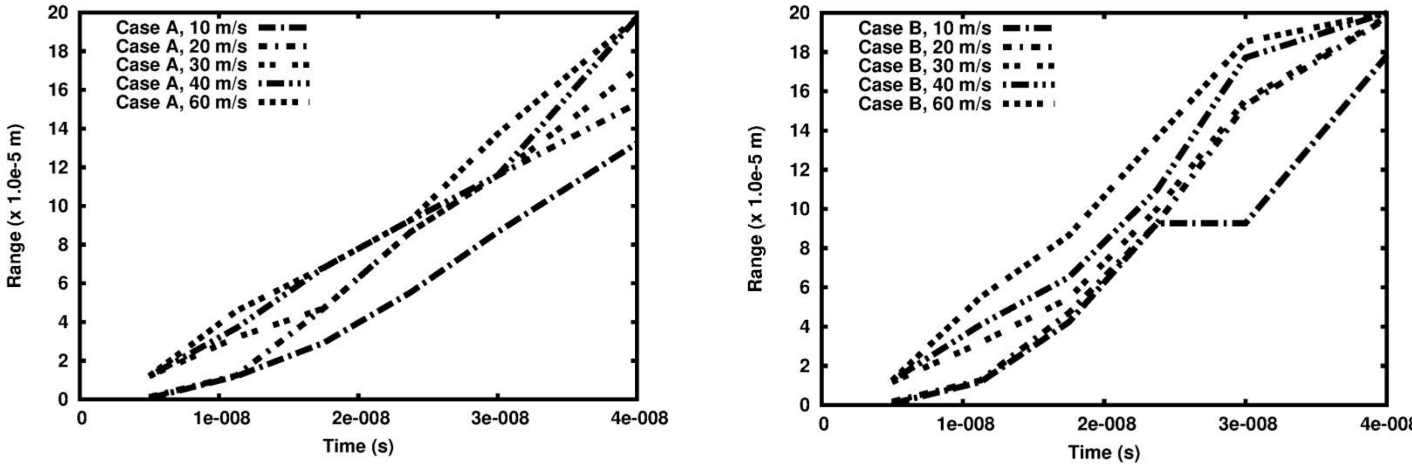

Damage advancement, the highest distance of a point of d>0.8 from the hitting edge: (**a**) Case A; (**b**) Case B.

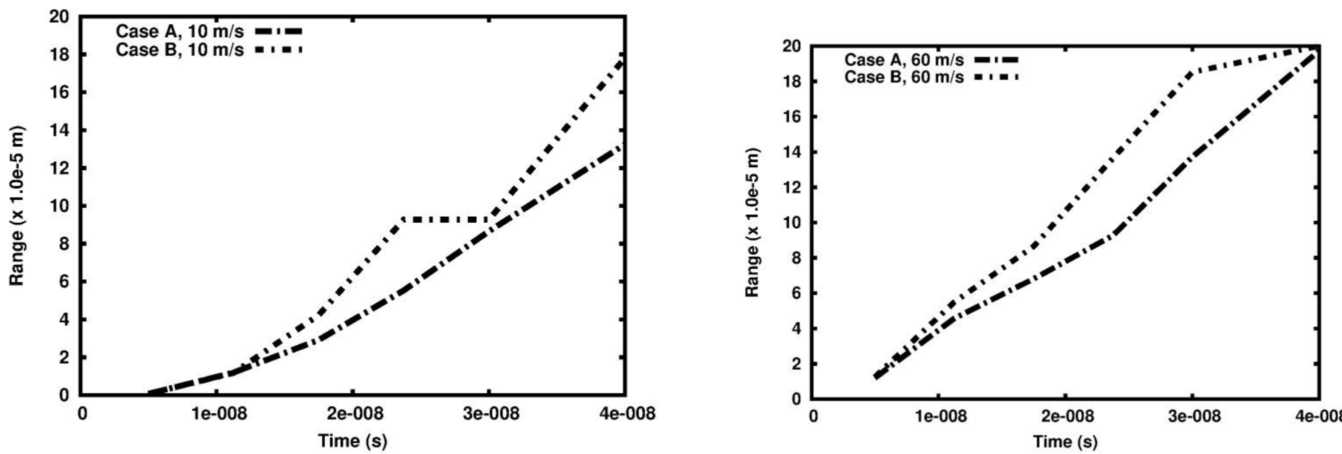

Damage advancement, the highest distance of a point of d>0.8 from the hitting edge, microstructure comparison: (a) impact velocity 10 m/s; (b) impact velocity 60 m/s.

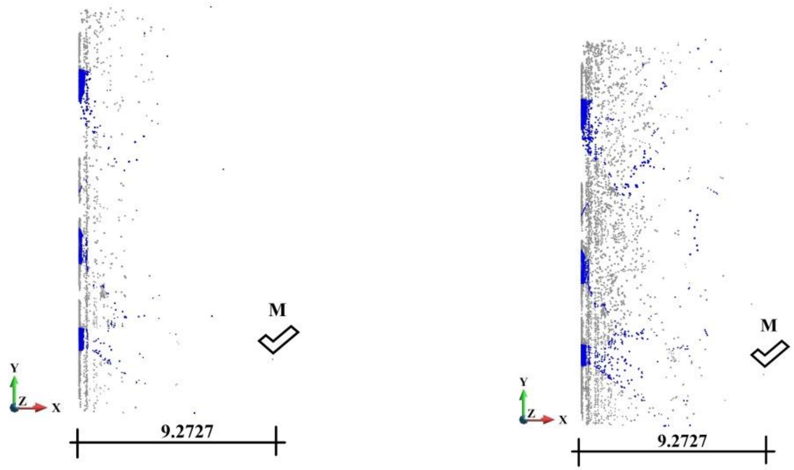

Damage advancement (dimension x 1.0E-5 m), the highest distance of a point of d>0.8 from the hitting edge at the impact velocity 10 m/s: (**a**) time 2.375e-8 s ; (**b**) time 3.000e-8 s.

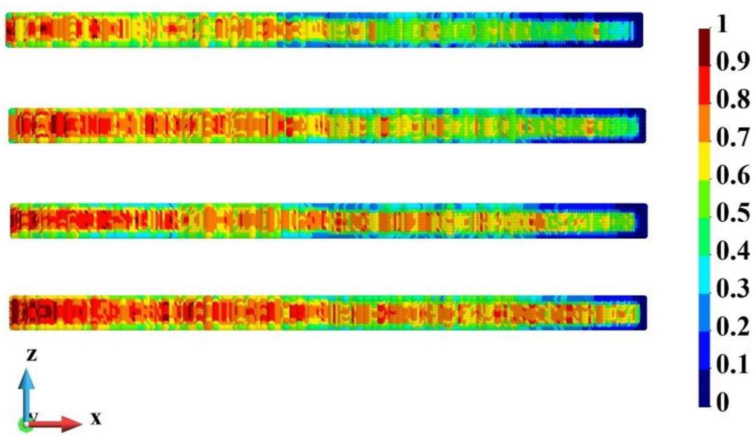

Comparison of damage variable distributions in the cross-section of the plate along x-axis at the mid-span of the plate, from the top: Case A, impact velocity 30 m/s, Case A, impact velocity 60 m/s, Case B, impact velocity 30 m/s and Case B, impact velocity 60 m/s.

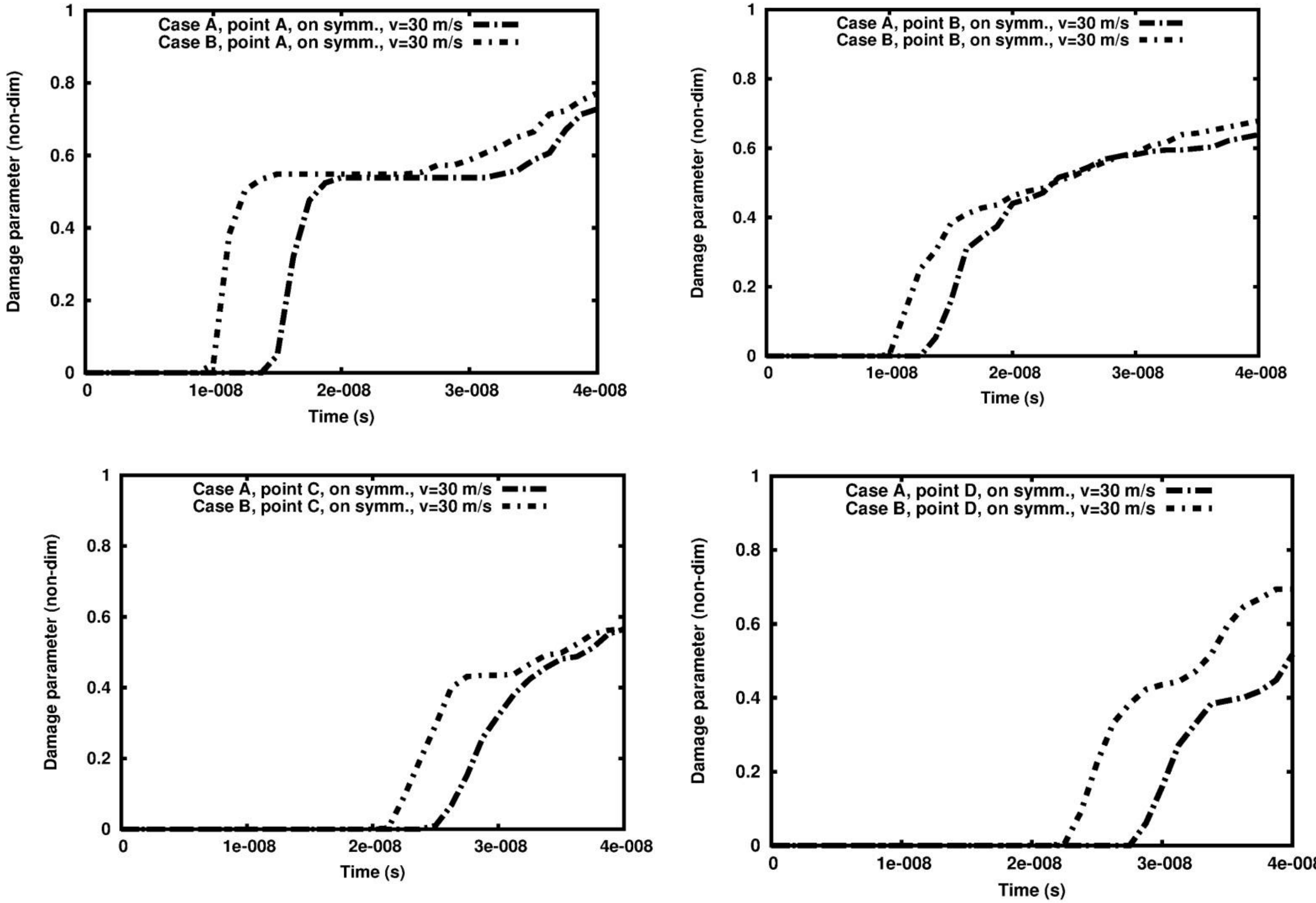

Comparison of variations of damage variable in time for Case A and B at different points: (**a**) Point A; (**b**) Point B; (**c**) Point C; (**d**) Point D.

Damage in Case B starts later

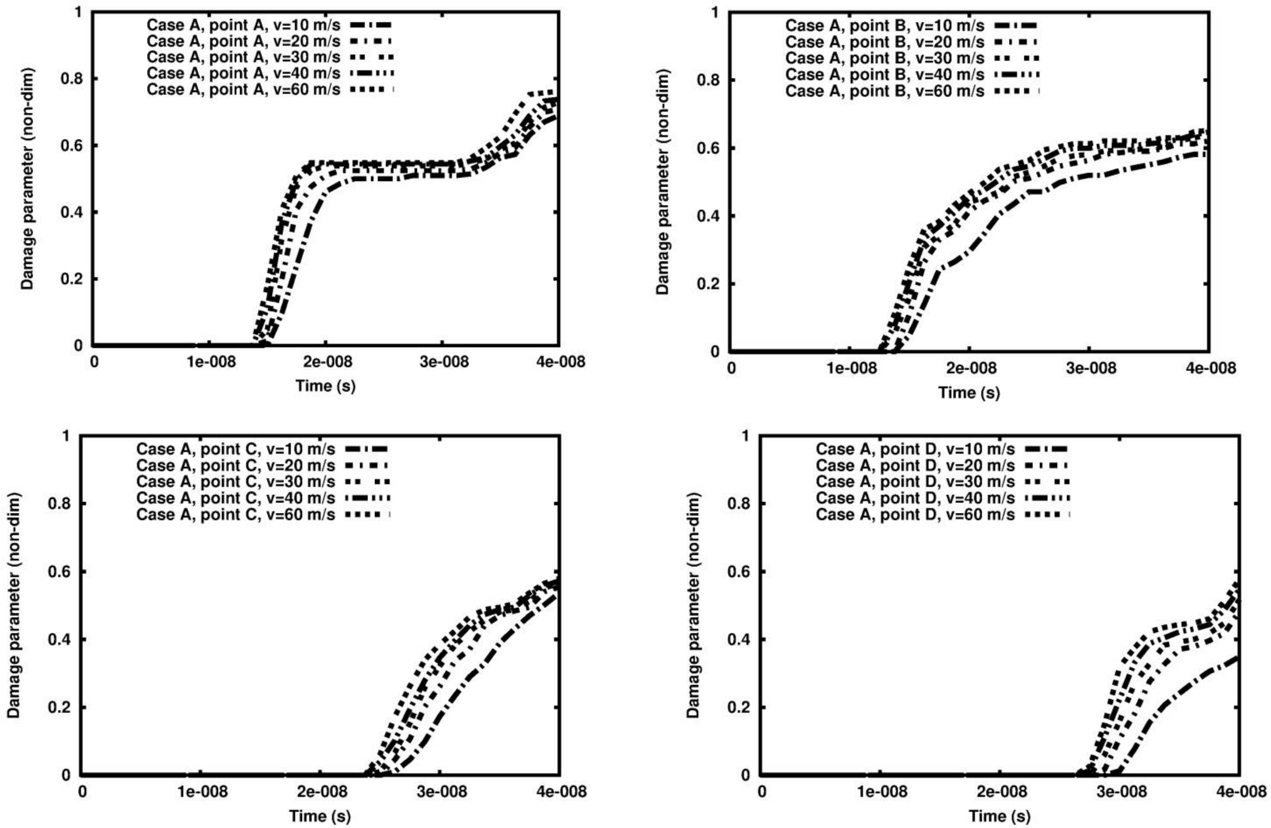

. Variation of damage variable in time for different impact velocities, Case A: (**a**) Point A; (**b**), Point B; (**c**) Point C; (**d**) Point D.

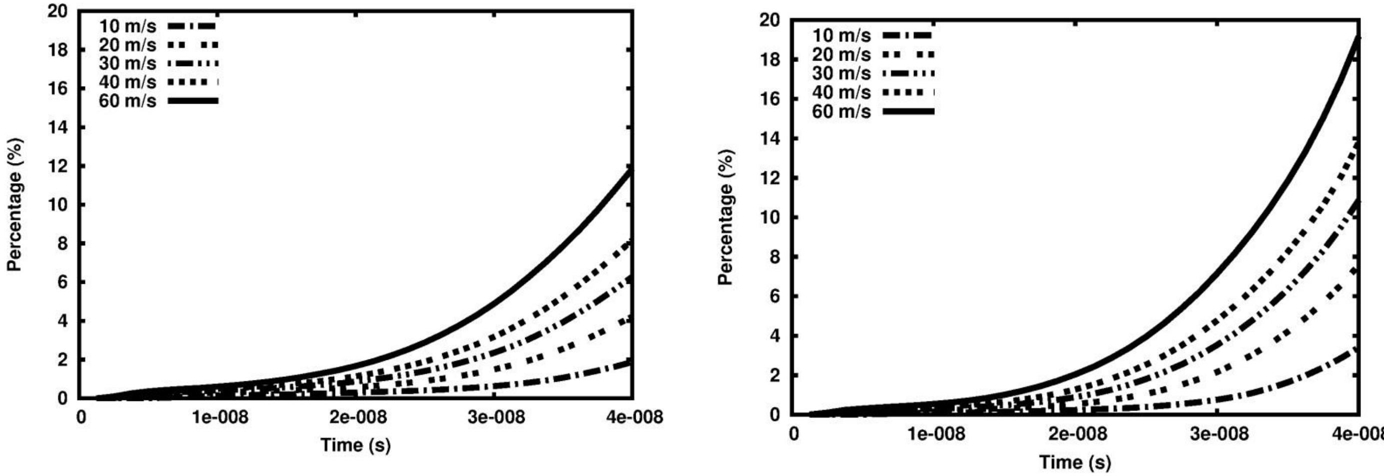

Variation of percentage of total damage in time for different impact velocities: (**a**) Case A; (**b**), Case B.

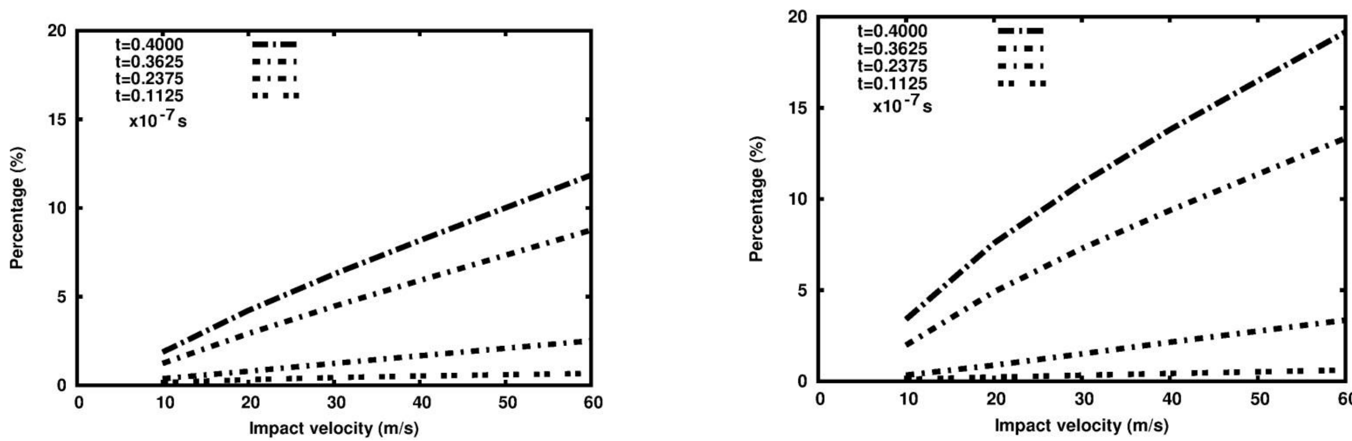

Dependence of percentage of total damage at particular time instants on impact velocity: (**a**) Case A; (**b**), Case B.

Following the considerations, we summarize and arrive at the conclusions as follows:

- Damage analysis of the impacting plates should be performed in three-dimensions,
- Damage is concentrated close to the mid-span of the depth of the cross-section and is the lowest close to the surfaces of the plates,
- Damage growth during impact that is characterized by percentage of total damage of the plate is strongly nonlinear,
- Damage appears early at sparse distributed points well before damage front where the damage becomes massive,
- At least in the investigated impact velocity range, the traces of damage appears practically in the entire plate independently of the impact velocity what means that almost the entire plate appears to be damaged to the different extent,
- When taking into account total damage variation dependence on impact velocity, the damage variation is almost linear at particular time instants. The latter allows for the damage prediction for different impact velocities using linear interpolation.
- At the beginning of the process, damage forms lines that are parallel to the hitting edge. We concern the phenomenon as a characteristic feature of the damage process of thin ceramic platelets.

Material parameters:

Skeleton (**SiC**):

- Young's modulus: 430.0 GPa
- Poison's ratio: 0.75
- Mass density: 3200 kg/m3
- Fracture toughness: 4.1 MPa.(m)^(1/2)

Base and piston (**steel**):

- Young's modulus: 210.0E+09 Pa
- Poison's ratio: 0.3
- Mass density: 7800.0 kg/m3

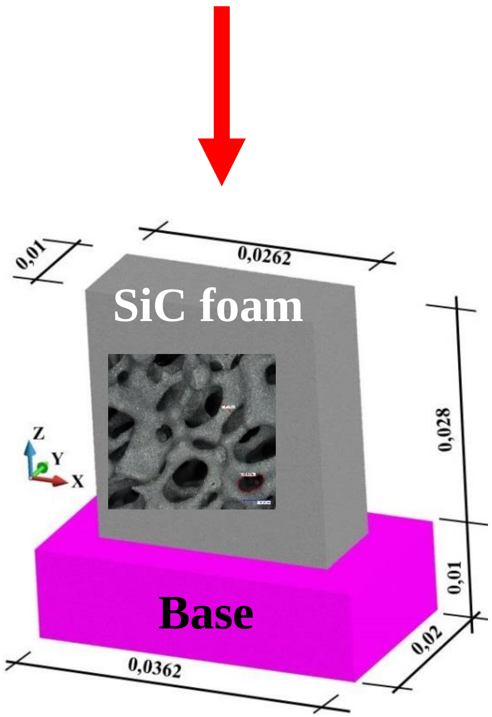

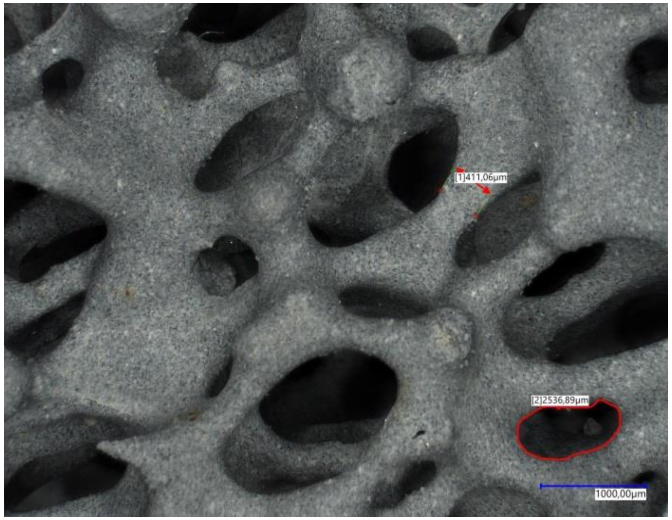

internal structure of the SiC foam

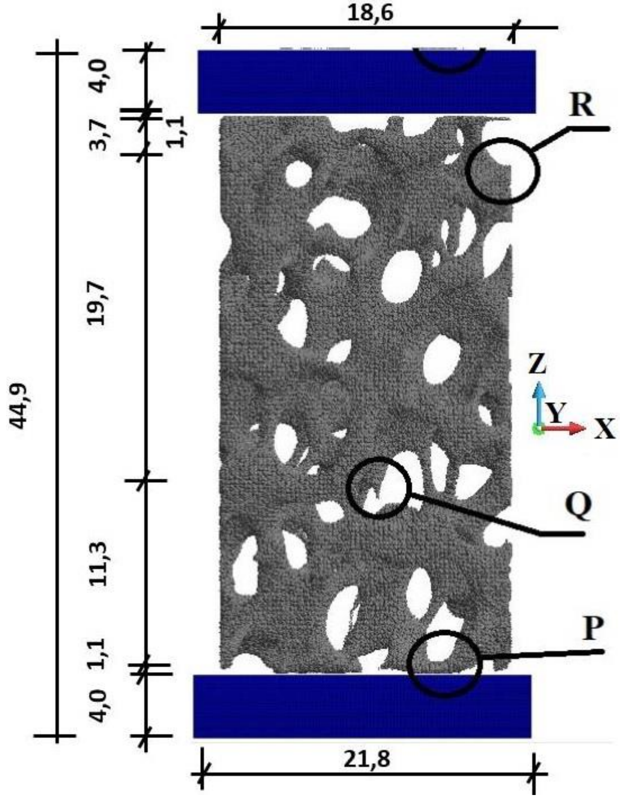

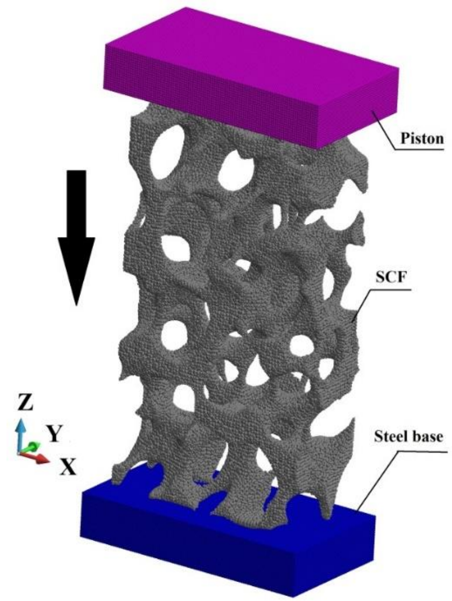

Discretization:
total 461,496 calculation points
Skeleton - 261,496
Base - 100,000
Piston - 100,000

Impact velocities:
40 m/s and 365 m/s

Critical stretch: SiC – 9.5716E-05

Horizon; skeleton: 30.0E-04 m, base and piston 6.0E-04 m
Process time: 3.06E-05, time increment 2.0e-08 s (below critical time), 1500 increments, solution time 3800 s, 1920 CPUs

Contact model – general contact, penalty formulation, friction coefficient 0.3

Base

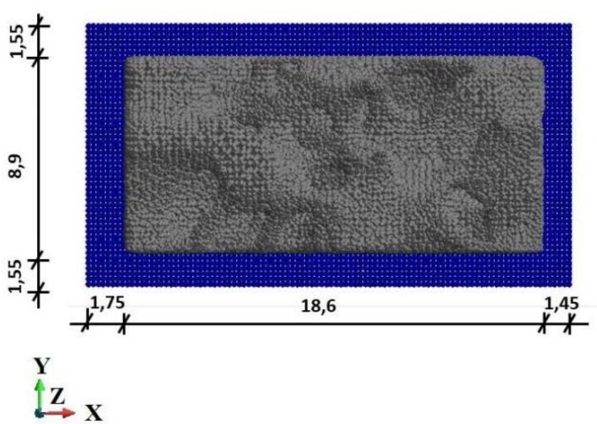

Positions of the points in the details: region P, region Q, region R

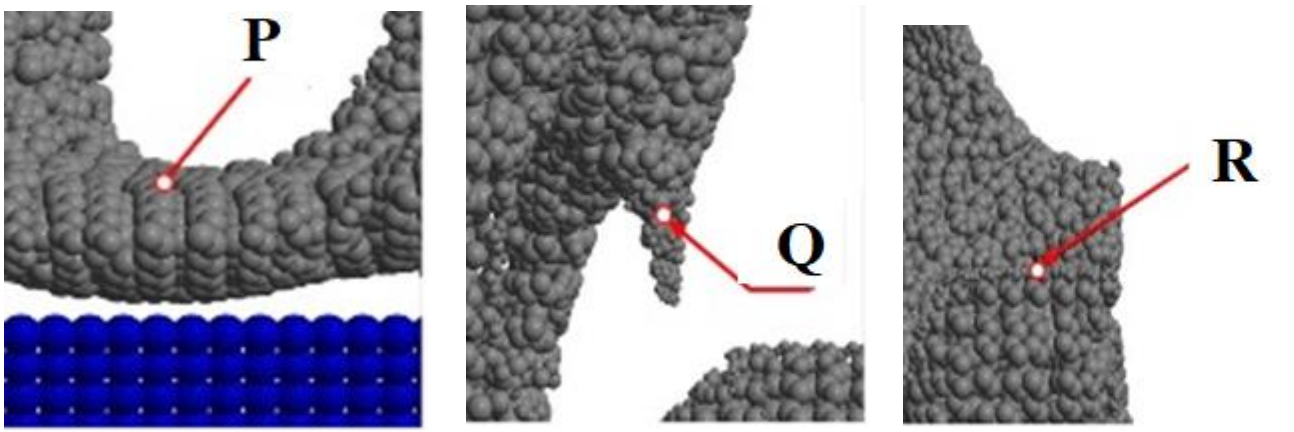

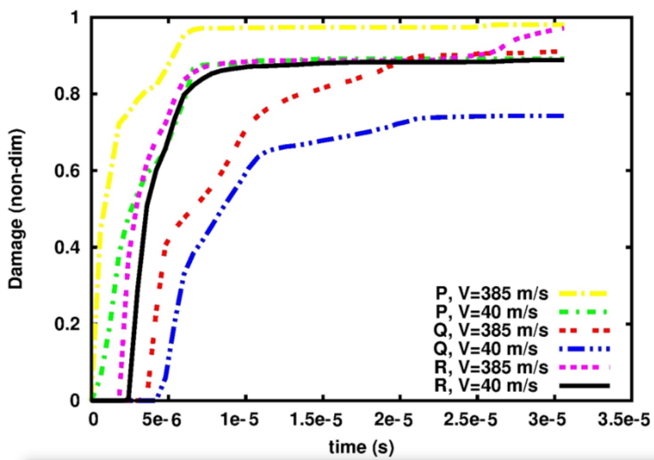

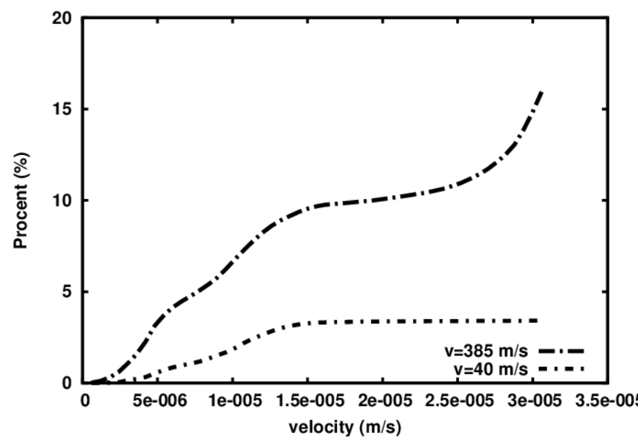

Total damage variation

Local damage (at points) variation

Numerical example

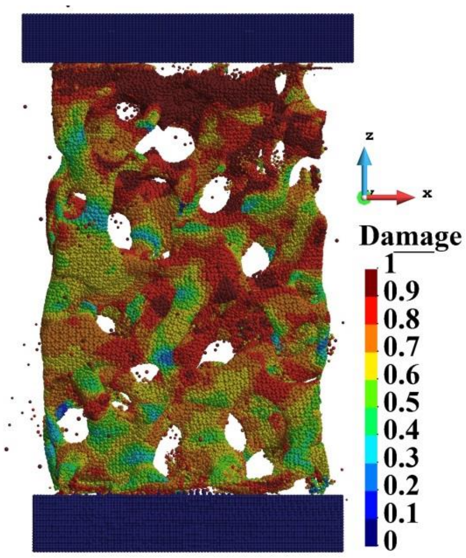

Points where d>0.95

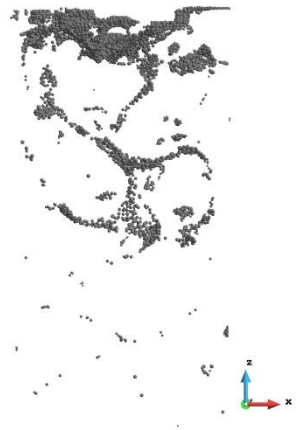

V=40 m/s, end of the process

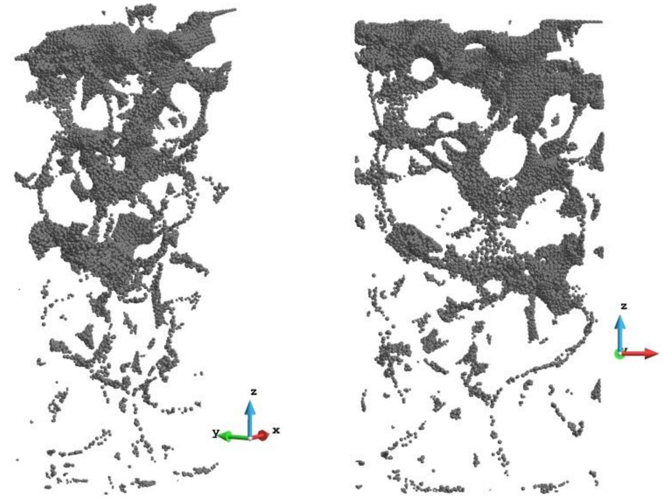

V=385 m/s

Points where d>0.95

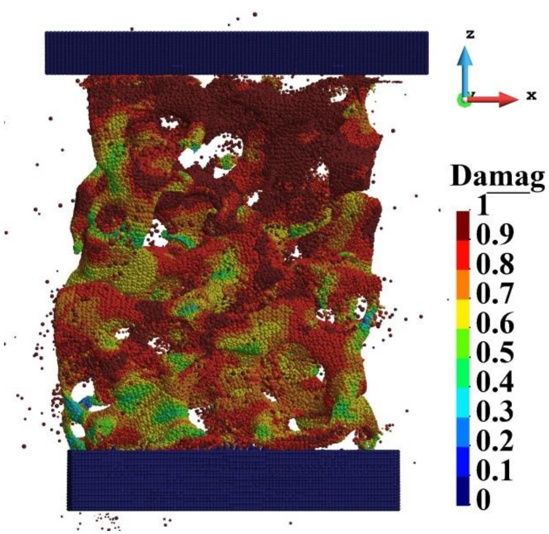

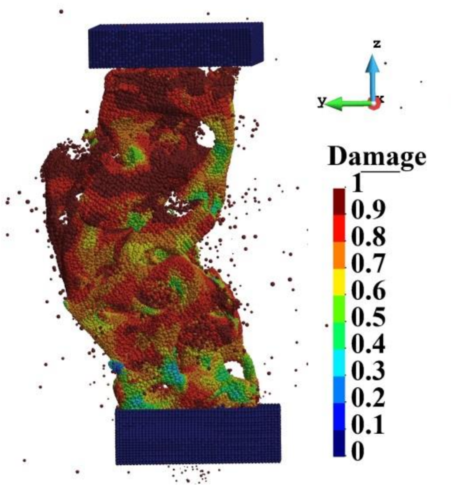

V=385 m/s, end of the process

- When the sample is subjected to the high-velocity impact, the structure undergoes self-contact in the pores.
- The destruction of the SCF into fragments of the structure appears in the course of a high-velocity impact.
- During high velocity process the self-contact appears.
- In the low-velocities impact, the damage of the structure is mainly due to local microcracks in the material.
- During high velocity impact appears out of plane failure mode.

5. Numerical model

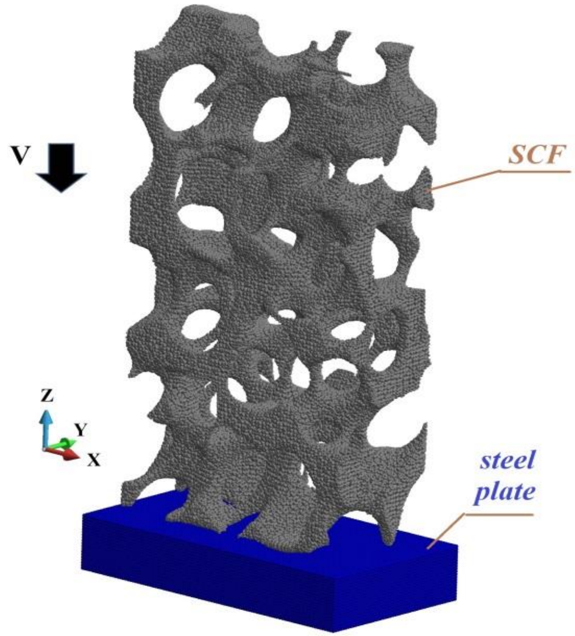

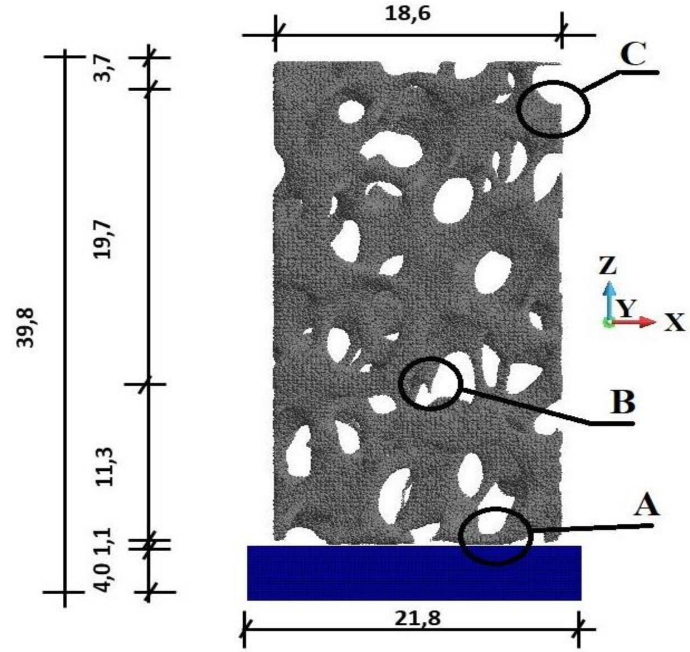

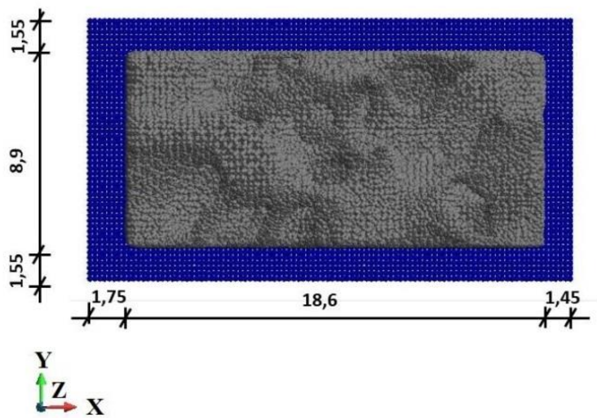

The **SCF sample** is discretized with 261,496 volumes, while the **steel base** counts 100,000 volumes.

In the calculations, the **horizon *h*** value for the:

- foam is assumed of 30.0E-04 m,
- base is 6.5E-04 m.

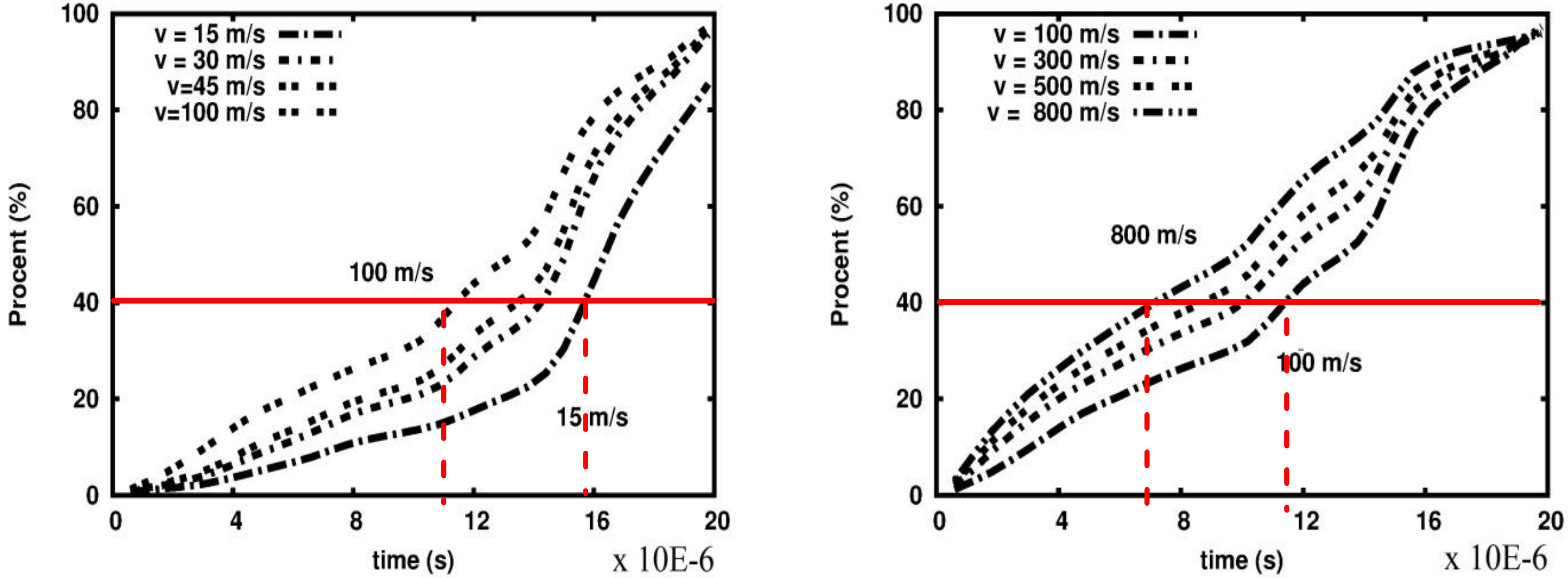

Percent of damage of the sample for low velocities, and for high velocities.

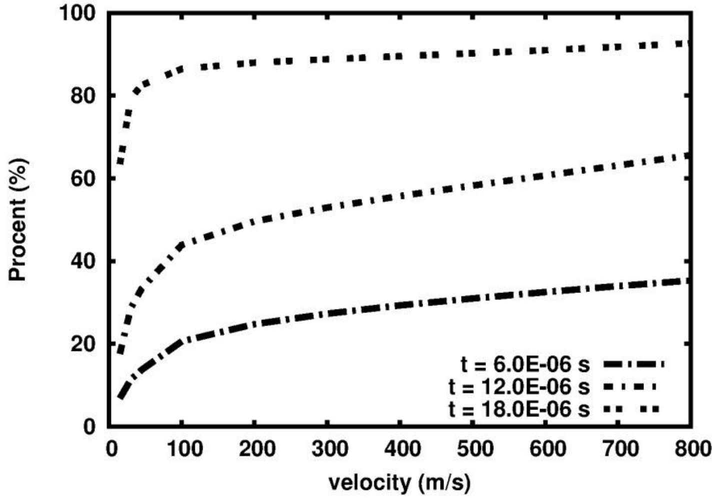

Percent of damage at the selected time instants.

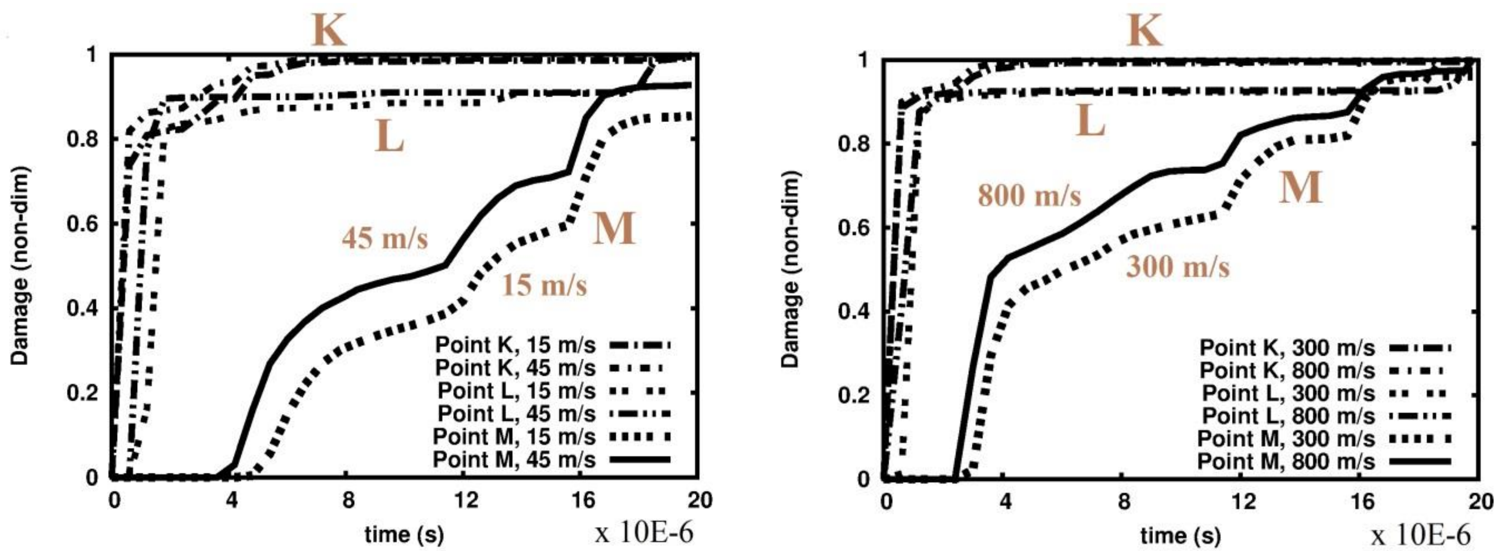

Damage at the observed points: low velocities, high velocities.

Low velocity impact

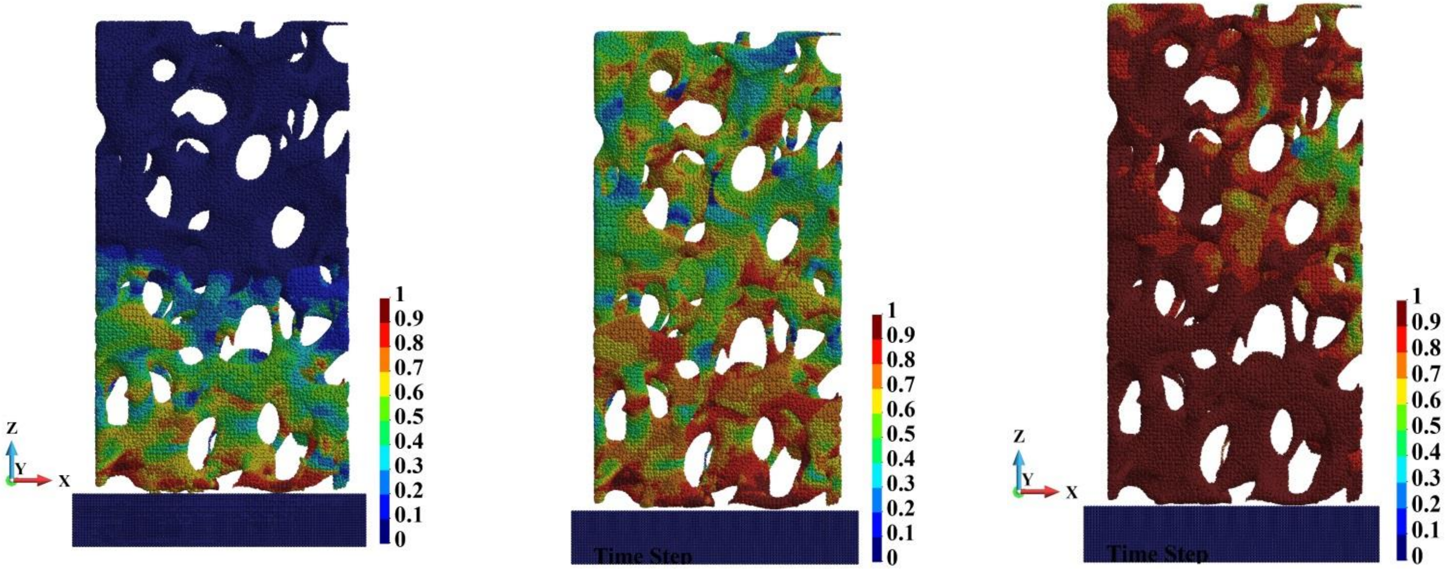

Impact velocity **15 m/s**, damage at time 2.4E-06 s, 11.4E-06 s , 19.8E-06 s

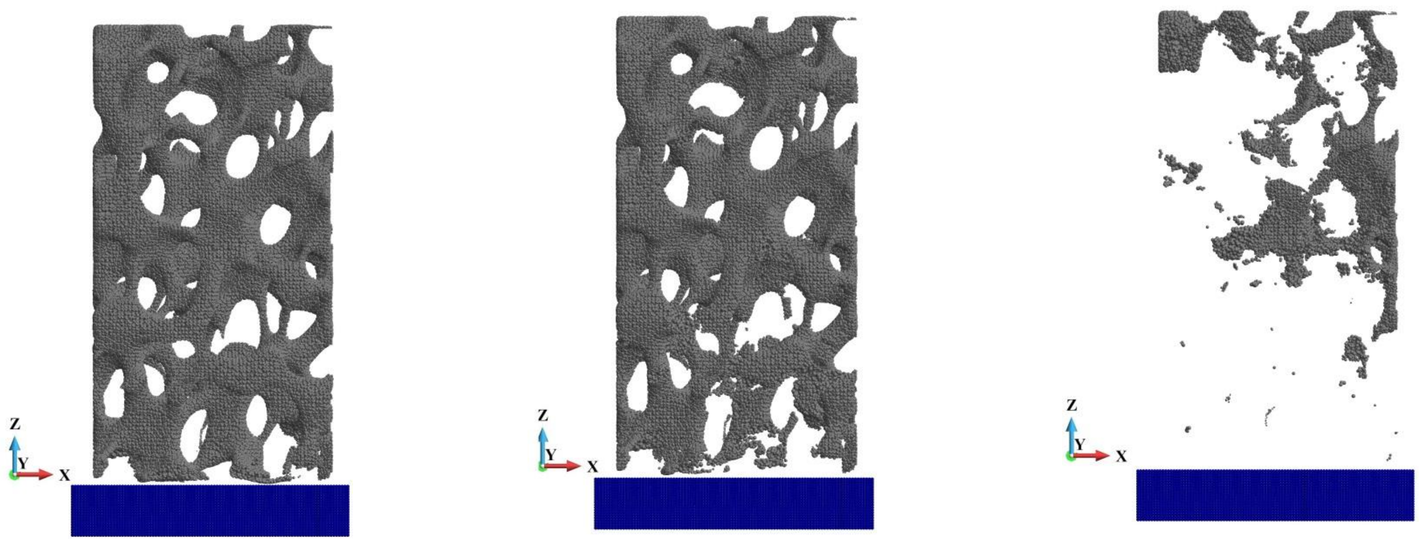

Impact velocity **15 m/s**, points of damage $d < 0.8$ at time 2.4E-06 s, 11.4E-06 s, 19.8E-06 s

High velocity impact

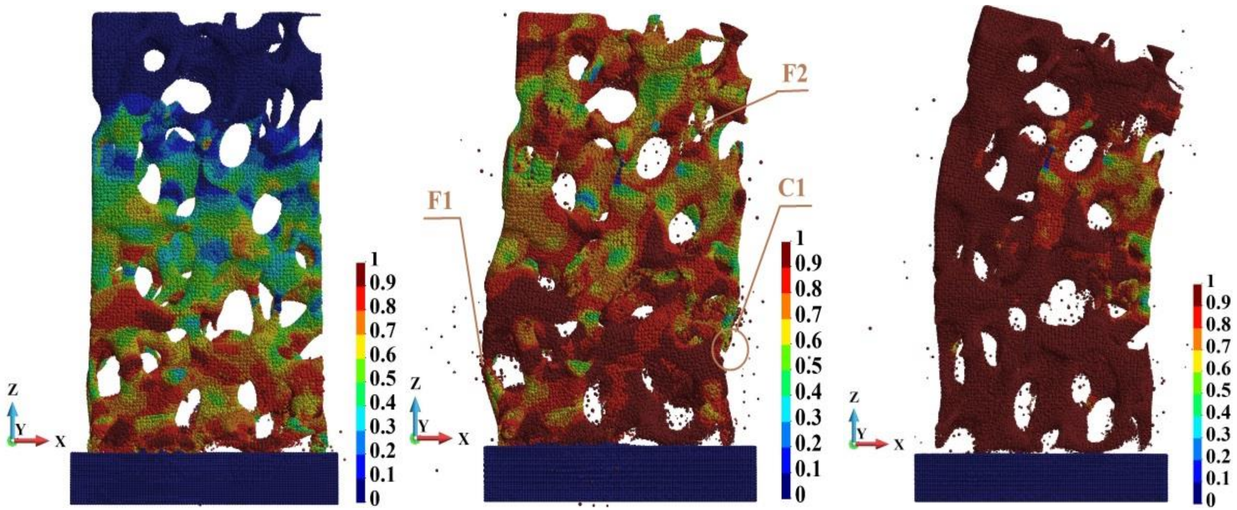

Impact velocity **800 m/s**, damage distribution at time 2.4E-06 s, 11.4E-06 s, 19.8E-06 s.

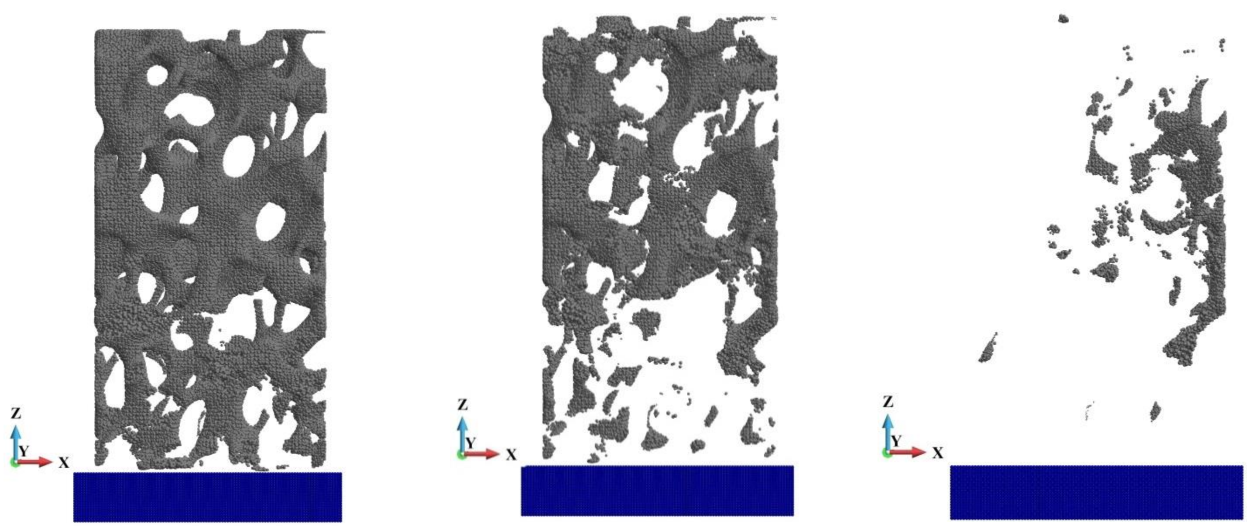

Impact velocity **800 m/s**, points of damage d < 0.8 at time 2.4E-06 s, 11.4E-06 s, 19.8E-06 s

A qualitative comparison of the high and low-velocity impact of a SiC foam has been presented in the paper. The analysis is performed using the peridynamics method. It has been found that the behaviour of the foam is different when the impact velocity is low in comparison to the high velocity response. The distinction of the low- and high-velocity process is based on evaluating total damage accumulation in the structure.

- In the high-velocities impact range, the total damage of the foam sample grows almost linearly with slight deviations from the linearity.
- When the foam sample is subjected to the high-velocity impact, the structure undergoes self-contact in the pores.
- The destruction of the SCF into fragments of the foam structure appears in the course of a high-velocity impact.
- While the impact is performer with the low-velocity, the fragmentation and self-contact does not appear.
- In the low-velocities impact, the damage of the foam structure is mainly due to local microcracks in the material.

Remarks on HPC

Number of processes and solution time for the adiabatic and coupled solutions.

Number of processes	Adiabatic solution		Coupled solution	
	Time (s)	Efficacy	Time (s)	Efficacy
4	5396	1	6362	1.00
8	2746	1.97	3248	1.96
16	1548	3.49	1879	3.39
24	1126	4.79	1335	4.77
32	1005	5.37	1199	5.31
48	777	6.94	935.0	6.80
96	733	7.36	837.0	7.60

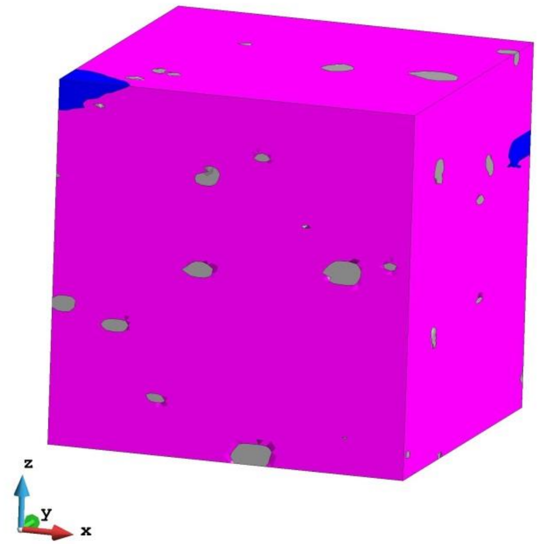

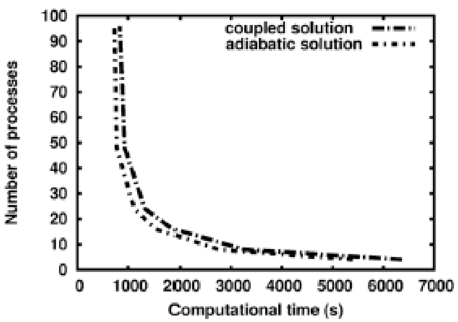

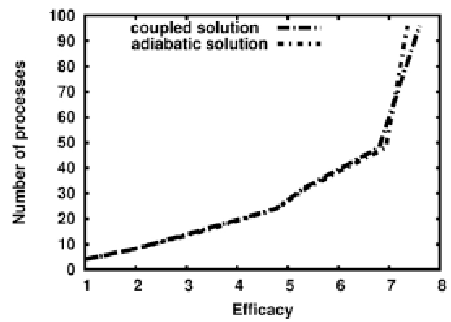

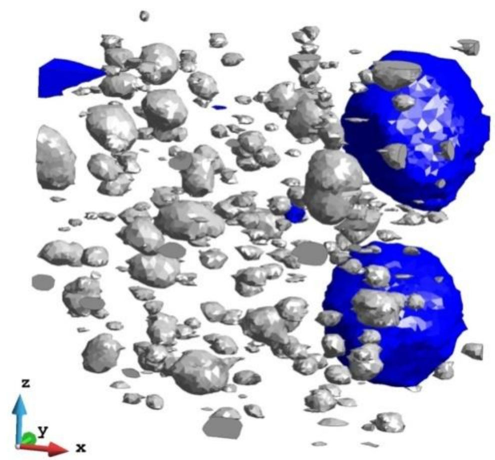

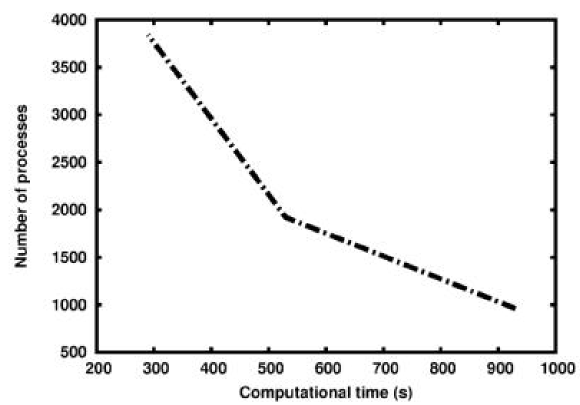

We used 960, 1920 and 3840 processes with the wall-clock times 930 s, 530 s and 290 s, respectively

The calculations were done using PL-GRID national computational resources at the Interdisciplinary Centre for Mathematical and Computational Modeling, University of Warsaw, the CYFRONET, Krakow, and Academic Computer Centre in Gdańsk, Poland.

1. Postek E., Sadowski T., Bieniaś J., *Simulation of impact and fragmentation of SiC skeleton*, Physical Mesomechanics, ISSN: 1029-9599, DOI: 10.1134/S102995992105009X, Vol.24, No.5, pp.578-587, **2021**
2. Postek E., Sadowski T., *Impact model of the Al2O3/ZrO2 composite by peridynamics*, COMPOSITE STRUCTURES, ISSN: 0263-8223, DOI: 10.1016/j.compstruct.2021.114071, Vol.271, pp.114071-1-12, **2021**
3. Postek E., Nowak Z., Pęcherski R.B., *Viscoplastic flow of functional cellular materials with use of peridynamics*, MECCANICA, ISSN: 0025-6455, DOI: 10.1007/s11012-021-01383-7, pp.1-18, **2021**
4. Postek E., Sadowski T., Boniecki M., *Impact of brittle composites: peridynamics modelling*, Materials Today: Proceedings, ISSN: 2214-7853, DOI: 10.1016/j.matpr.2020.12.511, Vol.45, pp.4268-4274, **2021**
5. Postek E., Sadowski T., *Thermomechanical effects during impact testing of WC/Co composite material*, COMPOSITE STRUCTURES, ISSN: 0263-8223, DOI: 10.1016/j.compstruct.2020.112054, Vol.241, pp.112054-1-25, **2020**
6. Postek E., Sadowski T., *High-velocity impact of 2-phase WC-Co composite plate - beginning of the process*, ARCHIVES OF METALLURGY AND MATERIALS, ISSN: 1733-3490, DOI: 10.24425/amm.2020.131726, Vol.65, No.1, pp.265-274, **2020**
7. Postek E., Sadowski T., *Temperature effects during impact testing of a two-phase metal-ceramic composite material*, Materials, ISSN: 1996-1944, DOI: 10.3390/ma12101629, Vol.12, No.10, pp.1629-1-13, **2019**
8. Postek E., Sadowski T., *Impact model of WC/Co composite*, COMPOSITE STRUCTURES, ISSN: 0263-8223, DOI: 10.1016/j.compstruct.2019.01.084, Vol.213, pp.231-242, **2019**
9. Postek E., Pęcherski R.B., Nowak Z., *Peridynamic simulation of crushing processes in copper open-cell foam*, ARCHIVES OF METALLURGY AND MATERIALS, ISSN: 1733-3490, DOI: 10.24425/amm.2019.130133, Vol.64, No.4, pp.1603-1610, **2019**
10. Postek E., Sadowski T., *Dynamic pulse sensitivity of WC/Co composite*, COMPOSITE STRUCTURES, ISSN: 0263-8223, DOI: 10.1016/j.compstruct.2017.10.092, Vol.203, pp.498-512, **2018**

Prerequisites for modelling

- grain size distribution,
- interface thickness distribution
- pore size distribution
- pore placement inside the material
- mechanical properties: Young modulus, Poisson coefficient, yield stress, material hardening, material viscosity